THE GEOLOGICAL SOCIETY
OF AMERICA®

Quantitative analysis of hillshed geomorphology and critical zone function: Raising the hillshed to watershed status

Zachary S. Brecheisen[1,†], Daniel D. Richter[1], Seulgi Moon[2], and Patrick N. Halpin[1]
[1]*Nicholas School of the Environment, Duke University, 9 Circuit Drive, Durham, North Carolina 27710, USA*
[2]*Department of Earth, Planetary, and Space Sciences, University of California–Los Angeles, 595 Charles Young Drive East, Los Angeles, California 90095, USA*

ABSTRACT

Landscapes are frequently delineated by nested watersheds and river networks ranked via stream orders. Landscapes have only recently been delineated by their interfluves and ridge networks, and ordered based on their ridge connectivity. There are, however, few studies that have quantitatively investigated the connections between interfluve networks and landscape morphology and environmental processes. Here, we ordered hillsheds using methods complementary to traditional watersheds, via a hierarchical ordering of interfluves, and we defined hillsheds to be landscape surfaces from which soil is shed by soil creep or any type of hillslope transport. With this approach, we demonstrated that hillsheds are most useful for analyses of landscape structure and processes. We ordered interfluve networks at the Calhoun Critical Zone Observatory (CZO), a North American Piedmont landscape, and demonstrated how interfluve networks and associated hillsheds are related to landscape geomorphology and processes of land management and land-use history, accelerated agricultural gully erosion, and bedrock weathering depth (i.e., regolith depth). Interfluve networks were ordered with an approach directly analogous to that first proposed for ordering streams and rivers by Robert Horton in the *GSA Bulletin* in 1945. At the Calhoun CZO, low-order hillsheds are numerous and dominate most of the observatory's ~190 km^2 area. Low-order hillsheds are relatively narrow with small individual areas, they have relatively steep slopes with high curvature, and they are relatively low in elevation. In contrast, high-order hillsheds are few, large in individual area, and relatively level at high elevation. Cultivation was historically abandoned by farmers on severely eroding low-order hillsheds, and in fact agriculture continues today only on high-order hillsheds. Low-order hillsheds have an order of magnitude greater intensity of gullying across the Calhoun CZO landscape than high-order hillsheds. In addition, although modeled regolith depth appears to be similar across hillshed orders on average, both maximum modeled regolith depth and spatial depth variability decrease as hillshed order increases. Land management, geomorphology, pedology, and studies of land-use change can benefit from this new approach pairing landscape structure and analyses.

INTRODUCTION

Hence the whole earth may be naturally divided into Basins or Dales, and also, by an independent division, into hills, each point of the surface belonging to a certain dale and also to a certain hill—James Clerk Maxwell (1870).

Interfluve and Hillshed Orders

In the intervening 150 yr since Maxwell's insights about hills and dales, the entirety of Earth's terrestrial surface has been mapped, studied, and managed, most often as river basins, stream networks, and nested catchments (Lehner and Grill, 2013; Strahler, 1957). Upland topography, however, has only recently been quantitatively investigated with regard to interfluve network connectivity and ordering (Scherler and Schwanghart, 2020a, 2020b). Our work seeks to describe and demonstrate hill or "hillshed" ordering (Evans, 2012; Maxwell, 1870) complementary to watersheds for natural landscape partitioning that can be used to conduct statistical analyses, perform environmental research, and improve land management. Whereas watersheds are connected by streams or rivers and are generally concave in structure, being bounded upslope by interfluves, hillsheds are convex, divergent, and include hilltop ridges (i.e., interfluves) bounded downslope by valleys and streams (Cayley, 1859), and they are usually bordered upslope by other hillsheds (Fig. 1). Watershed concepts inherently emphasize the importance of accumulative water flows and flow networks, whereas hillshed concepts focus on solid topographic structures and connected uplands across landscapes. Dendritic interfluves of connected upland topography can be ranked and networked using a Horton-Strahler stream-ordering approach (Horton, 1945; Scherler and Schwanghart, 2020a; Strahler, 1957), with hillsheds delineated by interfluves as they are bounded by streams, rivers, valleys, and neighboring hillsheds. Thus, first-order hillsheds, if not situated as isolated hills (Cayley, 1859), lead upslope to second-, third-, fourth-order, etc., hillsheds associated with increasing orders of interfluves (Fig. 1).

Interfluve and Hillshed Ordering and Critical Zone Science

Critical zone (CZ) science considers a geo-expanded ecosystem incorporating the full structure and function of the human-natural world, from the atmosphere and vegetation canopy, to Earth's surface down through soils, and into fractured and weathering bedrock (Brantley et al., 2007, 2016; Moon et al., 2017; Richter and Billings, 2015). To date, systematic landscape descriptions and analyses have mainly used hierarchical stream networks and nested watersheds to understand the hydro-biogeochemistry of Earth's CZ (Horton, 1945; Montgomery, 1999; Tarboton, 1996; Thorp and Delong, 1994; Vannote et al., 1980; Veltri et al., 1996). The zero- or first-order watershed is a de facto unit of study in many environmental studies, including CZ science (Brantley et al., 2016; Brecheisen et al., 2019b; Chorover et al., 2011; Godsey et al., 2018; Hasenmueller et al., 2017; Seyfried et al., 2018; Thorley et al., 2015; White et al., 2015; Wymore et al., 2017). This is logical

Zachary S. Brecheisen http://orcid.org/0000-0002-3712-1725
[†]zbrecheisen@gmail.com.

GSA Bulletin; https://doi.org/10.1130/B35724.1; 9 figures; 1 supplemental file.
Published online 17 December 2021

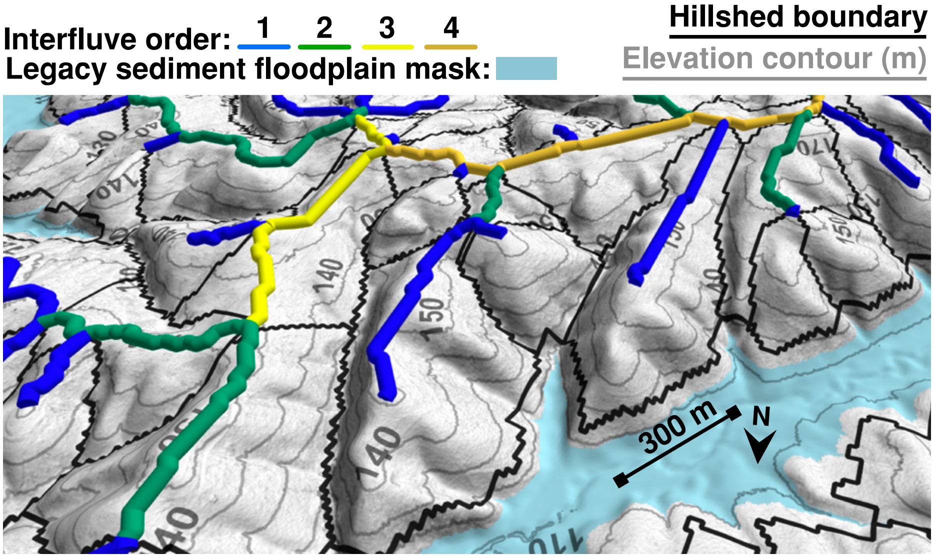

Figure 1. Topographic diagram of ordered interfluves and hillshed boundaries in Holcombe's Branch of the Calhoun Critical Zone Observatory (CZO). Interfluve orders are ranked and colored, as is the legacy sediment floodplain. Hillshed boundaries are black with labeled elevation contours (in m) in gray.

and appropriate for processes that correspond with relatively rapid advective water, sediment, and solute fluxes. However, many CZ questions, processes, and human land-use concerns feature the porous solid land surface and the structure or architecture and the evolution of the regolith itself. These features may well benefit from an analysis based on hillsheds in addition to analyses of watersheds.

Interfluves and their associated hillsheds are residual landforms that have not yet been eroded or dissolved away (Bos, 1971; Horton, 1945; Perron et al., 2009; Ruhe et al., 1967). As such, ordered interfluves and their hillsheds can be considered as discrete yet interconnected components of larger geomorphic dendrites (Cayley, 1859; Evans, 2012; Mark and Smith, 2004; Maxwell, 1870; Meerveld and Weiler, 2008; Scherler and Schwanghart, 2020a, 2020b). Trees and their branches have served stream and watershed approaches as meaningful metaphors in hydrology, and so too can a tree's twigs, branches, and trunk describe the distinct yet connected interfluves and hillsheds that are essential components to a landscape's geomorphology (Fig. 2).

Interfluves and their hillslopes are topographic features that subdivide watersheds, and their topology has a long history of research (Horton, 1945; Mark, 1979; Pfaltz, 1976; Scherler and Schwanghart, 2020a; Schneider, 2005; Warntz, 1975; Werner, 1972, 1988; Wilcox and Moellering, 1995). Werner's 1988 work initiated our concepts of ordered interfluve networks as interlocking antiparallel (i.e., parallel but with opposing directionality) to stream and river networks and provided a general methodology for the delineation of interfluve networks. Following Werner's interlocking interfluve-stream framework, we reasoned that landscapes, if their topography is inverted, should be amenable to interfluve delineation using the same digital elevation model (DEM)–based overland flow accumulation tools commonly used in hydrologic geographic information system (GIS) analyses to delineate streams and watersheds. Here, we present a hierarchical ordering of landscape topology via branching interfluves with discrete hillsheds for use in landscape geomorphometry. We discuss this approach by considering hillshed ordering with three examples of CZ processes. We assert that interfluve-hillshed ordering can be as useful to the study and management of the terrestrial environment as has been watershed ordering.

To introduce this approach, we quantitatively relate interfluve order to hillshed abundances, areas, elevations, slopes, and curvatures to characterize landscape geomorphology. Then, we apply the hierarchical ordering to patterns in three important CZ processes at the Calhoun Critical Zone Observatory (CZO) to demonstrate how interfluve and hillshed orders are related to: (1) historic and contemporary land-cover change (Brecheisen et al., 2019a, 2019b), (2) the magnitude of historic gully erosion linked to agriculture from the 1700s to 1930s (Brecheisen et al., 2019b; Brecheisen and Richter, 2021; Richter and Markewitz, 2001), and (3) spatially varying weathering depth modeled by topographic stress (Moon et al., 2017; St. Clair et al., 2015). We show that complex CZ processes affected by natural, social, and economic forcing mechanisms covary strongly with hillshed order.

METHODS

Derivation of Ordered Interfluve Networks and their Hillsheds

Several geomorphometric methods have been developed to delineate ridgelines, including a QGIS (QGIS Development Team, 2016) plugin for the delineation of topographic networks by Čučković (2016), the SAGA (Conrad et al., 2015) terrain analysis morphometry tool for valley and ridge detection (Rodriguez et al., 2002), and a polygon-breaking algorithm for ridge and valley network extraction that has been implemented in Grass GIS (Chang and Frigeri, 2002; Chang et al., 1998; GRASS Development Team, 2017).

Our approach sought to build upon existing geospatial tools for the delineation of streams and rivers from DEMs. This approach was chosen principally based on Werner's (1988) assertion that interfluve ridge networks must interlock with drainage networks. Though Werner employed a different methodology for ridge network extraction, it stood to reason that hydrological network delineation tools employed on inverted elevation terrain should yield the topographic counterpart to stream networks (i.e., interfluve networks). The terrain analyzed in this study was a DEM from Brecheisen and Richter (2021) that was processed to reverse the agricultural gullying that characterizes much of the microtopography of the Calhoun CZO landscape (Brecheisen et al., 2019b). That DEM that was ultimately derived from a 1-m-resolution 2014 Calhoun CZO light detection and ranging (LiDAR) DEM (available at OpenTopography.org [CCZO, 2014]).

Landscapes with ridgelines can be examined by inverting DEMs to generate interfluve networks using the same hydrologic GIS tools used to delineate stream networks. In this inverted terrain framework, interfluves are transformed into flow-accumulating linear features. Geospatial analyses, models, and figures in this study were generated and conducted using several software environments: R (Hijmans, 2020; R Core Team, 2020), ArcGIS (ESRI, 2016), TauDEM (Tarboton, 2015), and Whitebox Tools (Lindsay, 2019). The DEM was inverted by summing the minimum and maximum values of the DEM and then subtracting the DEM raster from this sum, resulting in a DEM with positive elevation values and the same minimum and maximum elevation values as the original DEM on an inverted terrain surface, following Equation 1:

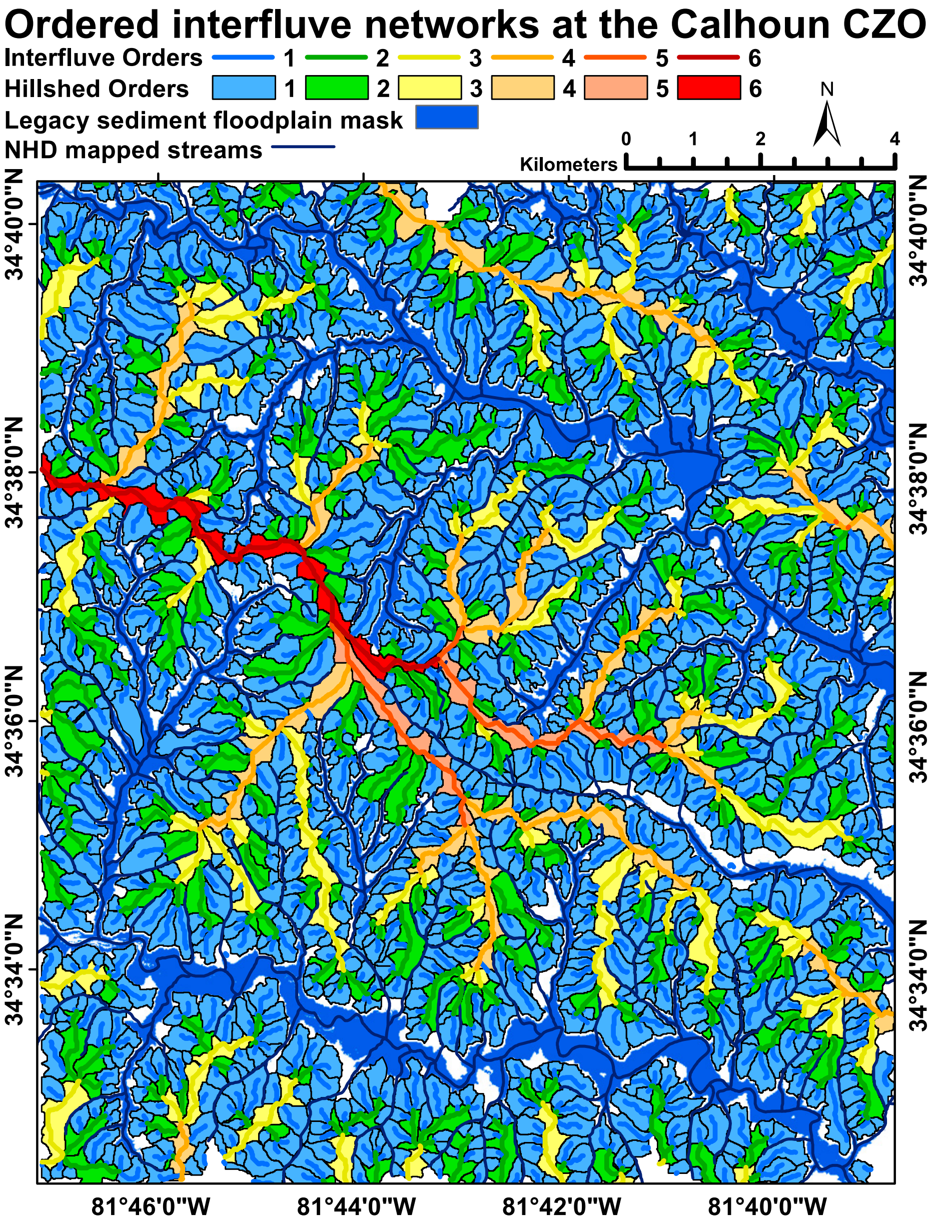

Figure 2. Ordered interfluve and corresponding hillshed map across the Calhoun Critical Zone Observatory (CZO). Interfluves and hillsheds are colored according to their Horton-Strahler ordering. The floodplain masks developed for hillshed delineation and National Hydrography Data set (NHD; U.S. Geological Survey, 2002) mapped streams are shown as dark-blue areas and lines, respectively.

$$DEM\_inv = [max(DEM) + min(DEM)] - DEM. \quad (1)$$

With only ~90 m of relief across the entire 190 km^2 Calhoun CZO landscape, interfluve delineation across relatively level and broad hilltops was challenging. To address this, we needed to consolidate spurious parallel flow accumulation lines into parsimonious interfluve networks via iterative flow-accumulation "burning" (Callow et al., 2007; Lindsay, 2016) of the inverted DEM. In this way, hillslope relief was increased along interfluves in order to enforce parsimonious single-line flow-accumulation network generation. The general procedure is: invert the topography, burn the interfluve "channels," delineate and label sub-hillsheds, assign hillshed orders, calculate topology, and merge the connected sub-hillshed components within orders. For clarity of reporting, the iterative DEM processing procedure implemented for interfluve network and hillshed delineation, the step by step methodology, and their reasoning are enumerated below. We recognize the great potential for method development of automated hillshed delineation from DEMs and freely disclose that the methodology below should be viewed as a general approach, where the particular numerical values chosen for resampling DEM data to focal statistic window sizes will undoubtedly need adjustment in other landscapes. We have not done sensitivity analyses for the effects of adjusting all of the different parameters below, but in cases where we have discovered potential pitfalls, we discuss their potential impacts.

(1) The 1-m-resolution smoothing via filling rough depressions (SvFRD) DEM from Brecheisen and Richter (2021) was inverted using Equation 1, then mean filtered in a 10 m window, and then resampled to 10 m resolution using Whitebox Tools in QGIS (Lindsay, 2019). Mean filtering smoothed any residual microtopographic roughness, likely from anthropogenic influences like agricultural terraces and road cuts (Brecheisen et al., 2019b). Resampling to 10 m DEM resolution greatly reduced the computational burden and processing time via 100-fold file size reduction. Though coarser in resolution, 10 m pixel resolution maintained high topographic DEM resolution across the ~190 km^2 Calhoun CZO landscape and yielded accurate terrain metrics (Grieve et al., 2016).

(2) Using TauDEM (Tarboton, 2015), the inverted DEM was sequentially pit-filled and processed for D-8 flow direction determination, and then D-8 contributing area was calculated across the Calhoun CZO. D-8 flow direction considers the elevation of a given pixel or cell in a raster DEM and considers it relative to its eight neighboring cells (four to the sides and four diagonal). Hydrologic flow direction for each cell is determined to be in the direction of the single neighboring cell which has the lowest elevation relative to the center. Based on the flow direction determination, flow accumulation can be determined on the basis of which cells flow into and out of each other yielding simple drainage networks. This TauDEM processing sequence was employed several times in this procedure and is hereafter referred to as "TauDEM D-8 flow analyses." In our approach, at each iteration of inverted flow-accumulation analysis, the standard pit-filling algorithms of TauDEM or Whitebox Tools were implemented such that the elevations of pit pixels were raised or backfilled to match the elevation of their outlet pixels. This resulted in small pit areas being filled but not to the extent that saddles were bridged.

(3) In order to concentrate contributing area (i.e., flow accumulation) along single-channel interfluves, the natural logarithm of the inverted

DEM D-8 contributing area raster was calculated and passed through a 45 × 45 cell mean filter. The log-mean-filtered contributing area raster was subtracted from the inverted 10-m-resolution DEM. The process of elevation subtraction along concentrated flow features is referred to as "stream burning" (Callow et al., 2007; Lindsay, 2016), but it was made more gradual here with less sharp DEM incision using the mean filter. Log-transformation was necessary to rescale the original flow-accumulation raster, ranging from zero to hundreds of thousands of contributing cells, into a range that could be subtracted from the DEM without yielding extremely negative values. The use of such a large filter invariably spanned the boundaries of different hillsheds and interfluves, but at this stage, our intention was simply to consolidate flow across inverted topography into parsimonious interfluve networks across broad uplands and eliminate spurious parallel forks. The final interfluve network or hillshed boundaries will be delineated in a subsequent step.

(4) The resulting inverted and burned DEM was reiterated for TauDEM D-8 flow analyses to yield a preliminary binary interfluve network with values >90 cells = 1 (potential interfluve pixel) and <90 cells = 0 (non-interfluve pixel). Here, a value of 90 flow-accumulation cells corresponded to 0.9 ha of the contributing area in the inverted DEM. This yielded a more spatially extensive interfluve network than the final network and will be subsequently refined and pruned in the next step.

(5) The above process yielded many parallel lines in the preliminary interfluve network across broad and level uplands. Many of the parallel lines were in close proximity and so were merged together via "line thickening" using a maximum filter on the binary raster within a 3 × 3 window. The resulting binary raster was then processed for line thinning and one iteration of spur removal. Spur removal functions to remove distal branches in linear network rasters. Having only one iteration of spur removal means that only the most distal branches were removed. All of these processes implemented in Whitebox Tools (Lindsay, 2019) function to condense and prune the branches of the preliminary interfluve network.

(6) In order to steepen the broadest and most leveled parts of the landscape to further concentrate simulated flow accumulation into single channels across the inverted DEM, the Euclidean distance from the refined interfluve network was calculated and divided by 25 to rescale the raster for the same purpose as in step 3. This raster was then manipulated such that it was simultaneously added to and subtracted from the inverted DEM from step 3. In this way inverted DEM pixels further from the refined interfluve network gained elevation, and pixels nearer to the interfluve network lost elevation proportional to their Euclidean distance from the binary network, thus steepening the inverted landscape. This was done in order to eliminate parallel channel artifacts. Determination of DEM processing for flow across flats and local minima reduction were handled by TauDEM's flow direction flat-resolution and pit-filling tools, respectively. If given too much weight when added to the inverted DEM, the Euclidean distance raster can result in hillshed borders being delineated incorrectly outside of valleys, and care should be taken in their use.

(7) The above inverted, channelized, and steepened DEM raster was reiterated for TauDEM D-8 flow analyses. A further refined "second draft" of the binary interfluve network was delineated as pixels with >450 cells (4.5 ha) contributing area, generally not including first-order interfluves and hillsheds. First-order hillsheds are narrowest with the highest local relief, and their interfluves are thus easiest to delineate in the absence of broader hilltops. These broad hilltops are found across the Calhoun CZO in areas with inverted flow accumulation >4.5 ha, across which it is difficult to delineate singular linear interfluve or ridge features, and so further "burning" was employed in these areas to concentrate simulated flow across these regions. This may not be necessary in landscapes with greater local relief.

(8) The second draft interfluve network was once more processed via maximum-filter line thickening, line thinning, and one iteration of spur removal in Whitebox Tools (2019). This refined second draft formed the final interfluve-burn network for the final stage of inverted DEM processing. The higher contributing area threshold in step 7 and pruning spur removal served to further distinguish and isolate high-order interfluve network branches across broad uplands.

(9) The original 10-m-resolution inverted DEM from step 1 was regenerated for final interfluve network delineation.

(10) Euclidean distance was calculated from the final interfluve-burn network in step 8.

(11) Traditional burning of the inverted DEM (Lindsay, 2016) was accomplished by subtracting 30 m elevation from all final interfluve-burn network pixels followed by Euclidean distance burning from the final interfluve-burn network once more as in step 6.

(12) The floodplain mask from Brecheisen and Richter (2021) was employed to mask mapped floodplain pixels in the inverted DEM across the Calhoun CZO to "NA." This was done because floodplains across the Calhoun CZO are characterized by 1.2–3 m deposition of postsettlement alluvial sediment rather than long-term landscape evolution that formed the upland interfluves and hillsheds of interest (Happ, 1945; James, 2013; Meade, 1982; Meade and Trimble, 1974; Trimble, 1975a, 1975b; Wade et al., 2020). In addition to having different geomorphic ontogeny, floodplains filled with recently eroded sediment (Wade et al., 2020) are extremely flat, making automated or manual hillshed delineation in these areas prone to error.

(13) For final interfluve network and hillshed delineation, the floodplain-masked, traditional + distance burned inverted DEM was processed a final time for D-8 flow analyses. D-8 flow analyses in this stage and subsequent hillshed delineation were conducted using Whitebox Tools (Lindsay, 2019). In this inverted topography, a "watershed" corresponds to a hillshed in normal topographic orientation, and thus watershed delineation tools were used to delineate hillsheds.

(14) Final interfluve network lines were delineated as inverted flow-accumulation pixels with >250 contributing cells (2.5 ha). Experimental watersheds that are monitored for stream flow in the Calhoun CZO's Holcombe's Branch (Fig. 1) are ~3–5 ha in area (Hodges et al., 2019), and our intent was to ensure that interfluves dividing drainages of this scale were mapped across the landscape, so a functional threshold of 2.5 ha was used. In other landscapes, if smaller (or larger) first-order interfluve ridge features are present, a different threshold value may be chosen. If values chosen are too low, however, interfluve lines may be delineated all the way down into bottomlands in some locations. Conversely, a threshold value that is too high will omit smaller ridges or divides. This is a problem in which ridge-extraction methodologies like those of Scherler and Schwanghart (2020a) may be advantageous, though they do not provide a means of hillshed delineation.

(15) The final resulting interfluve network raster was Strahler stream ordered (Strahler, 1957) and converted to a lines shapefile for figure generation using the "RasterStreamsToVector" function in Whitebox Tools (Lindsay, 2019).

(16) Individual nonnested hillsheds were delineated with unique identifier (ID) numbers across the Calhoun CZO using the "Subbasins" tool in Whitebox Tools with the binary final interfluve network raster and inverted D-8 flow direction raster from step 13 as inputs.

(17) Hillshed orders were determined across the Calhoun CZO using the "StrahlerOrderBasins" function with the same inputs as step 16.

(18) In order to tabulate the hillshed order branching sequence for each hillshed, the

"ConnectDown" tool in TauDEM was used in order to determine upslope hillshed ID branching connections. Connect "down" gives the upslope hillshed ID due to the terrain being inverted. For each individual hillshed, if the hillshed delineated uphill had the same Strahler order, they were both considered to be subcomponents of a single larger hillshed, and they were merged. This hillshed fragmentation occurred wherever interfluve network lines forked across the Calhoun CZO landscape. Though automated merging worked in most cases, there were some instances on hillsheds greater than third order in which the ConnectDown tool failed to correctly link subcomponents, likely due to some discrepancy between Whitebox Tools and TauDEM flow direction or pit-filling algorithms. In these cases, the hillshed subcomponents were identified for merging manually in ArcGIS and then merged in R.

(19) Using the upslope hillshed connection information, the Strahler orders of the first and second uphill hillshed junctions were determined for each hillshed. In total, for each hillshed, we tabulated: unique ID number, Strahler order, first upslope hillshed ID, second upslope hillshed ID, the first upslope connection hillshed Strahler order, and the second upslope connection hillshed Strahler order.

(20) Using the final raster of hillshed IDs, zonal statistics were calculated using the raster package in R (Hijmans, 2020; R Core Team, 2020) for each hillshed. Zonal hillshed statistics included geomorphic analyses of hillshed area (ha), median elevation (m), median slope (°), and median total curvature ($^{\circ*100}$/m) using Whitebox Tools (Lindsay, 2019) across the Calhoun CZO. Curvature values are reported in degrees multiplied by 100 in Whitebox Tools due to their small decimal values.

(21) The final step for hillshed data collation and map generation was to convert the hillshed ID raster into a polygon shapefile in order to merge all hillshed data in a GIS format. This also facilitated CZ application analyses of raster data sets with different spatial extents and resolutions than the original DEM. Hillshed polygons were rasterized to match the extent and alignment of raster data sets for land cover, soil gullying, and modeled weathering depth for statistical analyses using the fasterize package in R (Ross, 2020).

In this work, our inverted flow-accumulation procedure was structured to generate an interfluve network antiparallel (i.e., parallel but with opposing directionality) to and interlocking with the stream network (Werner, 1988) using the Calhoun CZO landscape. The final interfluve network (Figs. 1–3) was generated with an inverted DEM flow-accumulation threshold of 2.5 ha for first-order interfluves. We chose an inverted flow-accumulation threshold that yielded first-order interfluves that bounded the streams of our experimental watersheds mapped by the U.S. Geological Survey (U.S. Geological Survey, 2002). This was defined based on ongoing experimental field research in first-order watersheds within the Holcombe's Branch instrumentation and monitoring area of the Calhoun CZO (Hodges et al., 2019). Relief, climate, parent material, and landscape history (Dietrich et al., 1992; Perron et al., 2009; Scherler and Schwanghart, 2020a, 2020b) are contributing factors affecting both stream and interfluve delineation and will vary regionally (Tucker and Bras, 1998).

A hill or "hillshed" at the Calhoun CZO is here considered to end where the footslope meets the much more level floodplain identified via a sharp change in slope due to recently deposited eroded agricultural sediments (Fig. 1; Wade et al., 2020). Terminating the hillshed delineations in this way does break with Maxwell's 1870 assertion that any point on Earth's surface can be said to belong to both a hill and dale. Certainly, the argument can be made that floodplains are a part of the hills that have contributed sediment to them. Floodplains at the Calhoun CZO were inundated with sediment as a result of agriculturally accelerated upland erosion between the 1700s and early twentieth century (Brecheisen and Richter, 2021; Richter and Markewitz, 2001; Wade et al., 2020). As such, we excluded floodplain areas from hillshed mapping and statistical analyses because their formation and evolution did not result from the same long-term landscape evolution processes that shaped their surrounding hillslopes. Floodplain bottomlands were masked using analyses of deviation from mean elevation (Lindsay, 2019) from Brecheisen and Richter (2021). Masking eliminated sediment depositional areas spanning both very broad alluvial regions along major rivers corresponding to mapped wetlands (U.S. Fish and Wildlife Service, 1979–1994) as well as smaller sediment-filled tributary floodplains like those associated with historic mill dams and more modern sediment retention ponds across the Calhoun CZO (Walter and Merritts, 2008).

We used the final interfluve network and hillshed delineation (Figs. 1–2) to analyze landscape morphology, structure, and environmental processes across the Calhoun CZO. Our ordered interfluve networks of Calhoun CZO were compared to results generated from a newly developed approach for extracting and ordering ridges in TopoToolbox for MATLAB (Scherler and Schwanghart, 2020a; Supplemental Material, Figs. S1 and S2[1]). The functionality of TopoToolbox for ordering ridges (i.e., DIVIDEobj) was explored and provided for visual comparison in Figure S1, but we did not use the results from Matlab-based divide networks in our study. This is because first we found that the ordered-interfluve network results from both methods were qualitatively and quantitatively similar (Supplemental Material). Second, both methods still require the careful delineation of hillsheds following interfluve ordering, and thus most of the iterative "burn-in" procedure presented in this paper, or something analogous, would still be necessary to enable correct hillshed delineation. Last, our approach was based on open-source software readily available to people without software license restrictions. The details of the comparison and statistical assessments are described in Supplemental Material.

Connecting Hillshed Ordering to Geomorphic Characteristics and Processes

In this paper, we present examples of how hillshed ordering is associated with landscape structure and function. Three of these examples have observational data, including terrain geomorphometry, multidecadal land-cover change, and gully erosion intensity linked to historic agriculture. The fourth application uses three-dimensional geophysical modeling results for the bedrock weathering depth, calculated from the land surface to the bottom of fractured/weathered rock. The subsurface three-dimensional (3-D) stress fracture modeling results developed and published by Moon et al. (2017) were built upon the correspondence between two-dimensional P-wave seismic tomography and topographic stress by St. Clair et al. (2015).

The ordered hillshed is the basic unit of analyses in this study. Geomorphometric hillshed analyses were conducted via zonal statistics of 10-m-resolution terrain raster data derived from the same gully-filled SvFRD DEM (Brecheisen and Richter, 2021) used for hillshed delineation. Hillshed-ordered CZ analyses of raster data sets related to land cover, gully erosion, and bedrock weathering depth were conducted via rasterization of the hillshed polygon shapefile generated in hillshed delineation step 21. Rasterization

[1]Supplemental Material. Comparison of inverted terrain processing implemented in this study to TopoToolbox results for interfluve (ridge-line) extraction and hierarchical ordering. Different topographic curvature metrics are also explored at varying raster resolutions across hillshed orders. Please visit https://doi.org/10.1130/GSAB.S.16725133 to access the supplemental material, and contact editing@geosociety.org with any questions.

was accomplished using the fasterize package in R (Ross, 2020) to match the particular resolutions, extents, and alignments of those raster data sets. All geospatial data sets in this study were in projected Universal Transverse Mercator (UTM) zone 17N and North American Datum 1983 (NAD83).

Hillshed-Order Analyses of Landscape Geomorphology

All geomorphometric analyses were conducted on the gully-filled SvFRD DEM from Brecheisen and Richter (2021) resampled to 10 m resolution as outlined in step 1 in the delineation methodology. This eliminated the effect of microtopographic "noise" across meters (Brecheisen et al., 2019b) when considering landscape geomorphology across kilometers, yielding accurate terrain metrics (Grieve et al., 2016; Purinton and Bookhagen, 2017). Terrain analyses of ordered hillsheds included hillshed abundance, individual hillshed area (ha), cumulative landscape hillshed-order area (km^2), median hillshed elevation (m), median hillshed slope (°), and median hillshed total curvature ($^{\circ*100}$/m) (Evans and Cox, 1999; Lindsay, 2019). In this way, each hillshed served as an individual data point, with hillsheds grouped by interfluve order for terrain analyses. The resulting hillshed terrain data, except for abundance and total area, which are cumulative metrics, were analyzed via one-way analysis of variance (ANOVA) in R (R Core Team, 2020). Terrain attributes like curvature can be sensitive to DEM resolution (Deng et al., 2007). Though the effect of DEM resolution on terrain attributes was not a focus of this study, the effect of DEM resolution on terrain curvature was explored via analyses of median hillshed total curvature, plan curvature, and profile curvature at 1 m, 10 m, and 50 m pixel resolutions, with the results reported in Figure S3 (see footnote 1).

Land-Cover Change and Management as a Function of Hillshed Order

The second example of hillshed ordering involved land-cover analyses of land management between 1933 and 2014. Landscape analyses entailed a subset of the Calhoun CZO delineated by hillshed order for the estimation of percent coverage analyses of different hillshed orders for: 1933 and 2014 land cover, public versus private land areas in 2014 (U.S. Forest Service [USFS]), and land-cover transitions using the raster and landscape metrics packages in R (Hesselbarth et al., 2019; Hijmans, 2020; R Core Team, 2020). Land cover in 1933 was analyzed using mosaicked and georectified aerial photography, which is available on hydroshare.org as resource: 3edb9720a11845169dae4ba5b6212d27 (Brecheisen et al., 2019a, 2019b). To create a historic land-cover data set classified as forest, shrub/grass, and bare agricultural fields, 89 panchromatic photographs taken during the aerial survey in 1933 were scanned at 1200 dots per inch (dpi) resolution, georectified, color balanced, seam-lined, and mosaicked in ArcGIS 10.2.2 at ~0.5 m pixel resolution (Brecheisen et al., 2019a). The 1933 imagery raster was then classified into bare, grass/shrub, or forested land cover following Coughlan et al. (2017) and Brecheisen et al. (2019b). The classified raster was then down-sampled to 30 m resolution following the convention of the National Land Cover Database (Homer et al., 2015) using "majority" pixel land-cover assignment, whereby each new coarser pixel value is equal to that of the most abundant land-cover type within the original finer-resolution raster. This reduced processing times and filtered out "single tree" forest pixels.

Land cover in 2014 was classified using a 1-m-pixel-resolution canopy height raster derived by subtracting the July 2014 LiDAR (CCZO, 2014) ground DEM from the first-return DEM and removing the most extreme values (0–2.5th and 97.5–100th percentiles). For comparison to 1933 land cover, the 2014 LiDAR canopy height raster was aggregated into land-cover categories of pasture/hayfield or grass (0–1 m), recently harvested young forest (1–5 m), and intermediate or mature forest (>5 m). The resulting three-class canopy height raster was down-sampled to 30 m using nearest-neighbor interpolation in ArcGIS 10.2.2 (ESRI, 2016). In this case, nearest-neighbor interpolation was used because it preserved the nearest original categorical values for each pixel, which were based on continuous numerical tree-height data. An additional data set of the Calhoun CZO landscape within the boundaries of the 2014 LiDAR (CCZO, 2014) was generated as either publicly or privately owned in 2014 by converting USFS vector data (USFS, 2016) into a 30 m binary raster format.

In 1933, the entire landscape and Calhoun CZO was privately owned. By 1946, the USFS had purchased ~90% of the land that now forms the Enoree District of the Sumter National Forest. Last, a land-cover change transition matrix was generated with possible transitions being from either 1933 forested (F) or nonforested (NF) to 2014 forested (F) or nonforested (NF), giving four possible outcomes: F-F (continuously forested), F-NF (net deforested), NF-NF (continuously nonforested), or NF-F (net reforested). This matrix was used to explore land-cover changes over time.

Agricultural Gullying of the South Carolina Piedmont

The landscape spatial gully-volume distribution was analyzed following gully mapping in work by Brecheisen and Richter (2021) using a 2014 LiDAR DEM (CCZO, 2014). In this work, terrain microtopographic roughness (Brecheisen et al., 2019b) was analyzed, gullies were identified, and pregully surfaces were estimated in order to estimate gully depths and volumes across the landscape. The resulting gully-volume raster was subdivided into zones for each of the individual hillsheds and converted to gullied mass assuming a bulk density of 1.3 t/m^3. Within each hillshed, the total sum of gully-eroded soil was tallied, divided by individual hillshed area (ha) to yield hillshed estimates of gully intensity, and analyzed via ANOVA in R (Hijmans, 2020; R Core Team, 2020). The sum of eroded soil was also aggregated within hillshed orders for total landscape erosion estimation with and without area normalization.

Regolith Depth as a Function of Hillshed Order

Recent research on the patterns of bedrock weathering depth, both in theoretical predictions, e.g., Anderson et al. (2013), Lebedeva and Brantley (2013), Rempe and Dietrich (2014), and Riebe et al. (2017), as well as geophysical measurements (Befus et al., 2011; Flinchum et al., 2018; Holbrook et al., 2014, 2019; St. Clair et al., 2015), suggests that the depth of the bedrock weathering zone may be related to topography and specifically to interfluves and drainage patterns. Subsurface weathering investigations partition 3-D topographic stress model results (St. Clair et al., 2015) across hillshed orders in order to understand spatial patterns in the depth and variation of the bottom boundary of weathered bedrock. Following the methodology used by St. Clair et al. (2015), Moon et al. (2017) generated and published 3-D topographic stress models in the Calhoun CZO using poly3D (Thomas, 1993), which were analyzed according to hillshed order. The underlying granite bedrock of the Calhoun CZO is under regional stresses that interact with more local stresses based on interfluve orientation and curvature, regolith thickness, and drainage density. Due to computational limitations in generating stress models, four areas within Holcombe's Branch watershed (Dialynas et al., 2016), totaling ~350 ha spanning first- through fifth-order hillsheds, were selected for modeling with ~9 m pixel resolution. The regolith depth was estimated from the ground surface to the isosurface of the least compressive stress value of 0.5 MPa (Moon et al., 2017). The least compressive stress values of 0.5 MPa correspond closely to ~4 km/s *P*-wave velocities measured in the field for unweathered, competent bedrock (St. Clair et al., 2015). Thus, 0.5 MPa is taken to represent the transition zone between weathered to unweathered bedrock in this site. Weathering depth analyses were carried out by aggregating the modeled raster pixel depth values within corresponding hillshed orders.

Hillshed-Order Connections as Drivers of Landscape Geomorphology

The branching sequences of interfluves and their hillsheds are important to landscape structure and processes as well as land management. Whether a first-order hillshed joins a second-, third-, fourth-, fifth-, or sixth-order hillshed may strongly influence the geomorphology of that hillshed. Figure 3B illustrates branching sequences of first-order interfluves joining either second-, third-, or fifth-order interfluves from left to right along Holcombe's Branch in the Calhoun CZO. Here, interfluves and hillsheds are designated by multidigit interfluve Strahler ordering. Single-digit interfluve orders denote the interfluve order of an individual hillshed, whereas three-digit interfluve orders denote the interfluve order of an individual hillshed in digit one and the interfluve orders of the subsequent two uphill junctions in digits two and three. Digits two and three can skip orders (e.g., interfluve orders 246 or 135), though each sequential digit must be greater than the preceding digit. A 231 interfluve is nonsensical as the third-to-first-order transition would be downhill on real terrain and not possible in our inverted terrain flow-accumulation procedure. In these analyses, if either the first or second uphill junctions for a given a hillshed were outside the DEM, a 0 value was entered for structuring statistical analyses. The highest-elevation terminal sixth-order interfluve and all connections to it were retained for analysis and denoted as 600, #60, and ##6 in three-digit ordering, with "#" representing integers less than 6. This ordering scheme provided the hierarchical landscape topology of each hillshed landform and facilitated hillshed data analyses.

Terrain analyses partitioning the landscape into three-digit ordered hillsheds were the same as single-digit analyses: hillshed abundance, individual hillshed area (ha), cumulative landscape hillshed-order area (km^2), median hillshed elevation (m), median hillshed slope (°), and median hillshed total curvature ($^{\circ*100}$/m). Median elevation for each ordered hillshed was further analyzed using multiple regression without interaction terms in R as a function of median hillshed slope, hillshed area, and one- or three-digit hillshed orders as explanatory factors. In these regression analyses, all hillsheds of fourth order or lower for which the first or second uphill junction was not a sixth order interfluve and that were outside the Calhoun CZO study area were omitted from analyses. With the exception of hillsheds connected to the sole sixth-order hillshed and that hillshed itself, if either the first or second uphill junctions for a given a hillshed were outside the DEM, they were excluded from linear model analyses by ANOVA or multiple regression or inclusion in cumulative abundance or area metrics.

RESULTS AND DISCUSSION

Terrain Analyses of Ordered Hillsheds

Terrain analyses focused on upland terrain (~89% of the Calhoun CZO landscape) and excluded floodplains and terraces (~11% of the landscape) that are inundated in legacy sediment from upslope agricultural erosion (Wade et al., 2020). Terrain analysis of hillshed abundances (Fig. 4A) indicated that 76.5% of all hillsheds are first order, 18.25% are second order, 4.2% are third order, 0.9% are fourth order, and 0.1% are fifth order, and the single partial sixth-order hillshed represents 0.05% of the total Calhoun CZO hillshed count. Conversely, hillshed order is positively related to individual hillshed area ($F[5,1747] = 293.6$, $p < 0.05$), as average individual hillshed area increases exponentially from 7.2 ha for first-order hillsheds to 165.1 ha for the sixth-order hillshed (Fig. 4B). Total upland area in each hillshed order across the 190 km^2 Calhoun CZO landscape is the product of these two patterns and is characterized by a more gradual decrease in cumulative area as interfluve order increases (Fig. 4C). First-order hillsheds total ~97 km^2, whereas fifth- and sixth-order hillsheds total only ~3.35 km^2. First-order hillsheds thus cover ~64.4%, second-order hillsheds cover ~19.2%, third-order hillsheds cover 9.2%, fourth-order hillsheds cover 5.0%, fifth-order hillsheds cover 1.1%, and the sixth-order hillshed represents 1.0% of the non-floodplain Calhoun CZO. Given that there is a single truncated sixth- order hillshed within the Calhoun CZO landscape, we retained the sixth-order hillshed data for graphical and statistical analyses, but we do not make broad inferences based on these results.

Median hillshed elevation, slope, and curvature are all strongly related to interfluve order. Median hillshed elevation is positively related to interfluve order ($F[5,1747] = 33.63$, $p < 0.05$) with first- to sixth-order hillsheds having median elevations of 142.5 m, 153.5 m, 155.4 m, 167.5 m, 173.6 m, and 179.4 m, respectively (Fig. 4D). The steepest slopes ($F[5,1747] = 39.34$, $p < 0.05$) and greatest total curvature terrain ($F[5,1747] = 18.87$, $p < 0.05$) are found on first-order hillsheds (median slope = 7.35°, median total curvature = 0.32$^{\circ*100}$/m) with interfluves becoming flatter and more level uphill as interfluve order increases (Figs. 4E–4F). We suggest this pattern is the result of long-term landscape evolution in which the hillslopes of most lower-order hillsheds have experienced increased diffusive soil creep and advective stream incision due to their proximity to major rivers (Dietrich et al., 1992; Fernandes and Dietrich, 1997; Montgomery and Dietrich, 1992; Perron, 2017; Perron et al., 2009; Scherler and Schwanghart, 2020a, 2020b). We infer that these processes, having driven landscape denudation in an unglaciated humid subtropical environment for millions of years (Bacon et al., 2012; Richter and Markewitz, 2001), have led to the spatial distribution of hillshed

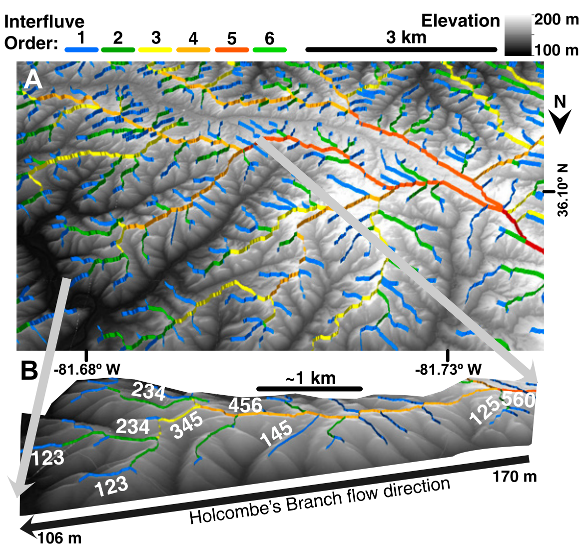

Figure 3. Three-dimensional representation of ordered interfluve networks (A) across the Calhoun Critical Zone Observatory (CZO) landscape and (B) zoomed in on the eastern half of Holcombe's Branch watershed, illustrating how the orders of interfluve connections and topology can be captured via multi-digit interfluve orders.

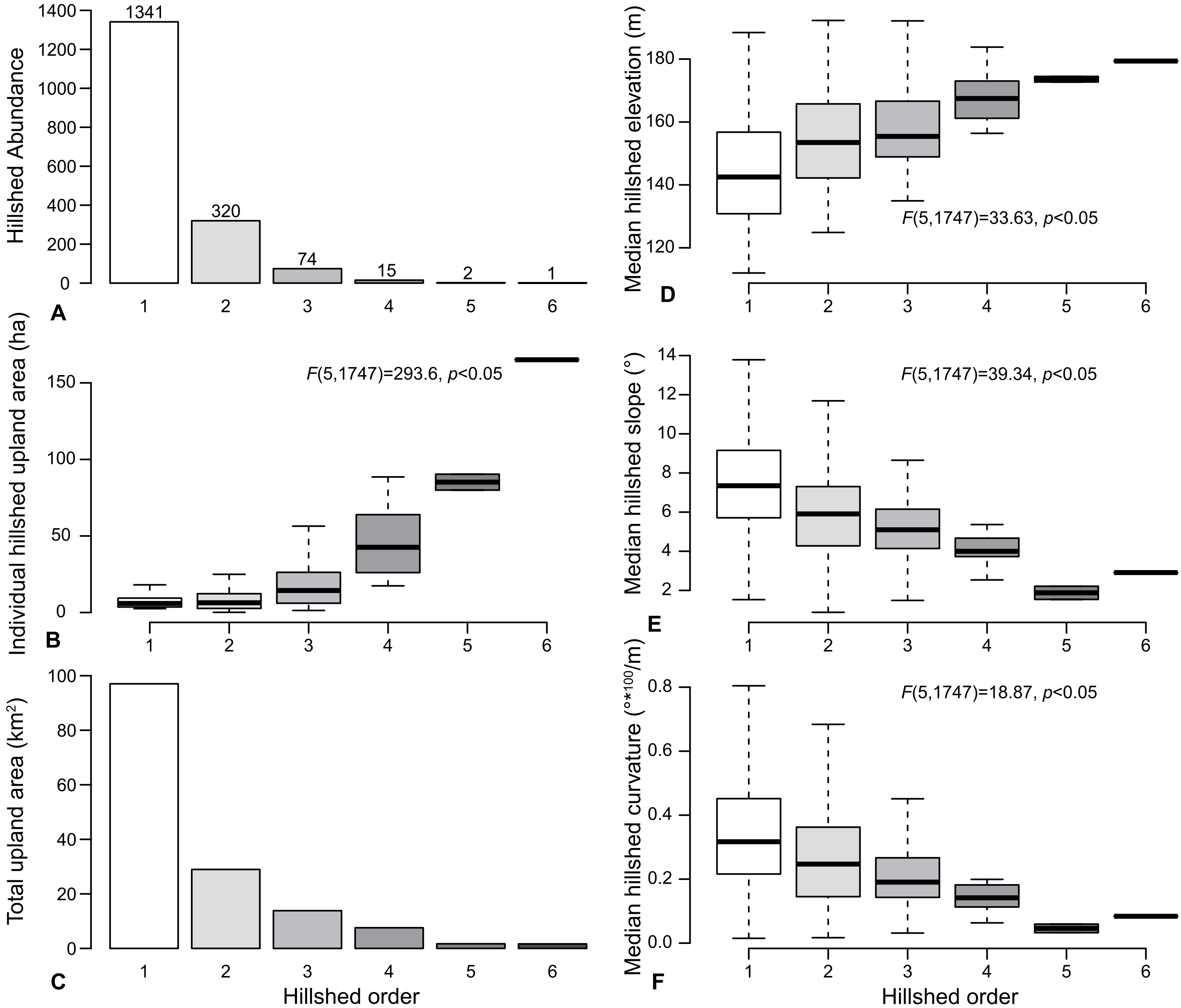

Figure 4. Single-digit interfluve ordering terrain zonal analyses of hillshed: (A) abundance, (B) area, (C) cumulative area, (D) median elevation, (E) median slope, and (F) median hillshed total curvature. The number of interfluves in each order is above each bar in the top abundance panel, and analysis of variance (ANOVA) *F*-test results are shown within area, elevation, slope, and curvature box plots. Terrain analyses were conducted on a 10-m-pixel-resolution mean-filtered and gully-filled digital elevation model from Brecheisen and Richter (2021).

elevation, steepness, and curvature across the landscape. A factor undoubtedly related to these processes is the influence of aspect, especially on narrow and steep first-order hillsheds, which may generally be considered to have two opposing hillslope faces. This is a promising area for future hillshed geomorphic research.

Though interfluve ordering of hillsheds yields insight into the structure and organization of topography, the potential utility is not limited to analyzing landscape geomorphology. The results of three CZ applications of interfluve ordering follow: (1) land-cover change, (2) agricultural gully erosion, and (3) regolith depth.

Land-Cover Change and Management as a Function of Hillshed Order

Low-order hillsheds were so seriously eroded and gullied by farming that, beginning in the mid-1930s, the USFS established the Sumter National Forest and purchased farms with degraded soils in need of “retirement” from many families who were in debt and defaulting on taxes (Coughlan et al., 2017; Giesen, 2020; Hansen, 1991; Metz, 1958; Richter and Markewitz, 2001). As such, the majority of the Calhoun CZO landscape consisting of erosion-prone low-order hillsheds transitioned about a century ago from private to public ownership and is now managed for its forest cover and timber. Only the most productive lands, like those found on high-order hillsheds, were retained in private ownership

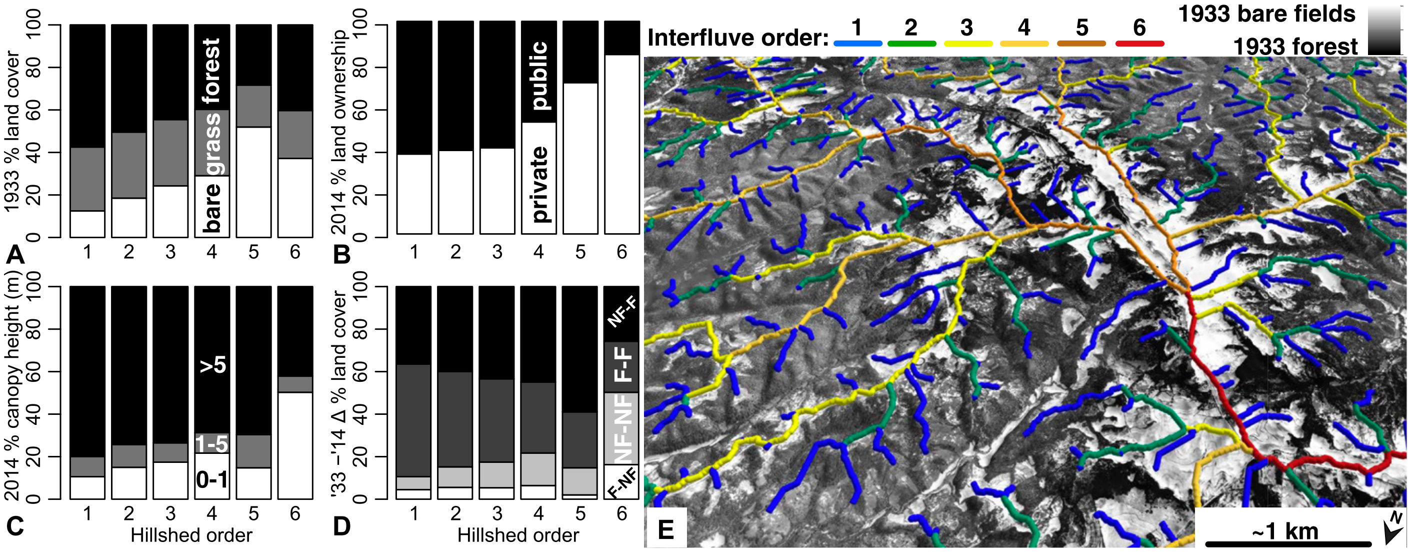

Figure 5. (A–D) Critical zone application bar plots of (A) land-cover percentages in 1933, (B) land ownership in 2014, (C) land-cover canopy height class percentages in 2014, and (D) land-cover change from 1933 to 2014. (E) Aerial three-dimensional view of the 1933 landscape's aerial photography overlain by interfluve orders. F—forested land cover; NF—nonforested land cover. Image is centered approximately on –81.72° longitude and 34.62° latitude.

(Metz, 1958; Richter and Markewitz, 2001). Land ownership change from private to public led to land-management changes. Reforestation expanded across the Sumter National Forest, as it did across the Southern Piedmont, especially on low-order interfluves.

Connections among hillshed order, area, slope, curvature, and erosion indicate that the history of land-use change at the Calhoun CZO maps well onto an ordered hillshed landscape framework. Historic 1933 land-cover patterns of percent bare cropland, grassy shrubland, and forest are strongly related to hillshed order, with bare exposed agricultural soil cover increasing as hillshed order increases up to fifth order as terrain becomes broader and flatter (Fig. 5A). The prominence of these patterns and connections between land-cover history and topographic networks provided the initial inspiration for this entire study (Fig. 5E).

Land ownership also maps well onto ordered hillsheds, with private land ownership most concentrated on high-order hillsheds, whereas the greatest proportions of public lands are on low-order hillsheds (Fig. 5B). Contemporary 2014 land cover also maps well onto hillshed orders, with the distribution of nonforest cover (0–1 m canopy height) increasing as hillshed order increases, and mature forest cover (>5 m canopy height) decreasing as hillshed order increases (Fig. 5C). Areas with net deforestation (F-NF) or prolonged nonforestation (NF-NF) are mainly on high-order hillsheds (Fig. 5E). Land cover on low-order hillsheds is more likely to have remained forested between 1933 and 2014 compared with higher-order hillsheds (F-F), following land ownership patterns (Coughlan et al., 2017).

Agricultural Gullying of the SC Piedmont

The Calhoun CZ and the entire Southern Piedmont have been subjected to some of the most severe agricultural erosion in the United States, which was most severe from the eighteenth century to early twentieth century. The deeply weathered soils and hillslopes were incised by gullies, and large quantities of soil eroded downslope during one to two centuries of intensive upland agriculture (Coughlan et al., 2017; Hansen, 1991; Richter and Markewitz, 2001; Trimble, 2008). The broadest interfluves of the Calhoun CZO landscape in the Southern Piedmont have remained biogeomorphically stable over geologic time, with erosion rates as low as 0.35–3 m/m.y. on a fifth-order hillshed prior to colonial settlement (Bacon et al., 2012). Because of this, Calhoun CZO soils and saprolite are deep and extremely weathered, with estimates of pedologic residence times more than 2–3 m.y. (Bacon et al., 2012). Anthropogenic land-cover and land-use change, converting largely forested areas to plowed fields and grazing lands, greatly enhanced soil erosion (Richter and Markewitz, 2001). In aggregate, gully-erosion volume estimates across the Calhoun CZO range from ~300 m^3/ha (Noto et al., 2017) to ~600 m^3/ha (Brecheisen and Richter, 2021).

ANOVA analysis of the mapped gully-erosion estimates from Brecheisen and Richter (2021) that span the entire Calhoun CZO landscape indicates that average gully-erosion intensity decreases as hillshed order increases from first to sixth order (Fig. 6). Lower-order hillsheds experienced significantly more soil loss by gulling than higher-order hillsheds ($F[5,1747] = 2.342$, $p = 0.0.039$; Fig. 6A). The most marginal lands, such as first-order interfluves, were possibly cultivated last and abandoned first due to intense erosion in the decades before the 1933 aerial imagery was acquired (Coughlan et al., 2017). Because first-order hillsheds dominate the landscape in terms of abundance and area, they contributed 79.1% of the total eroded soil mass from gullies across the landscape (Fig. 6B). After normalizing total eroded soil mass by total landscape hillshed area, a somewhat more gradual pattern emerges of decreasing gully-erosion intensity as hillshed order increases, though first-order hillsheds still have more than an order of magnitude greater gullying intensity than fourth-, fifth-, or sixth-order hillsheds (Fig. 6C).

Modeled Regolith Depth as a Function of Hillshed Order

Previous geophysical and drilling studies at the Calhoun CZO have revealed important interactions between regional and local stresses on deep weathering of bedrock (Moon et al., 2017; St. Clair et al., 2015). Here, we examined the relationship of hillshed order and weathering depth using published 3-D geophysical models from the Calhoun CZO (Moon et al., 2017; St. Clair et al., 2015). Two-dimensional bedrock weathering depth profiles at the site

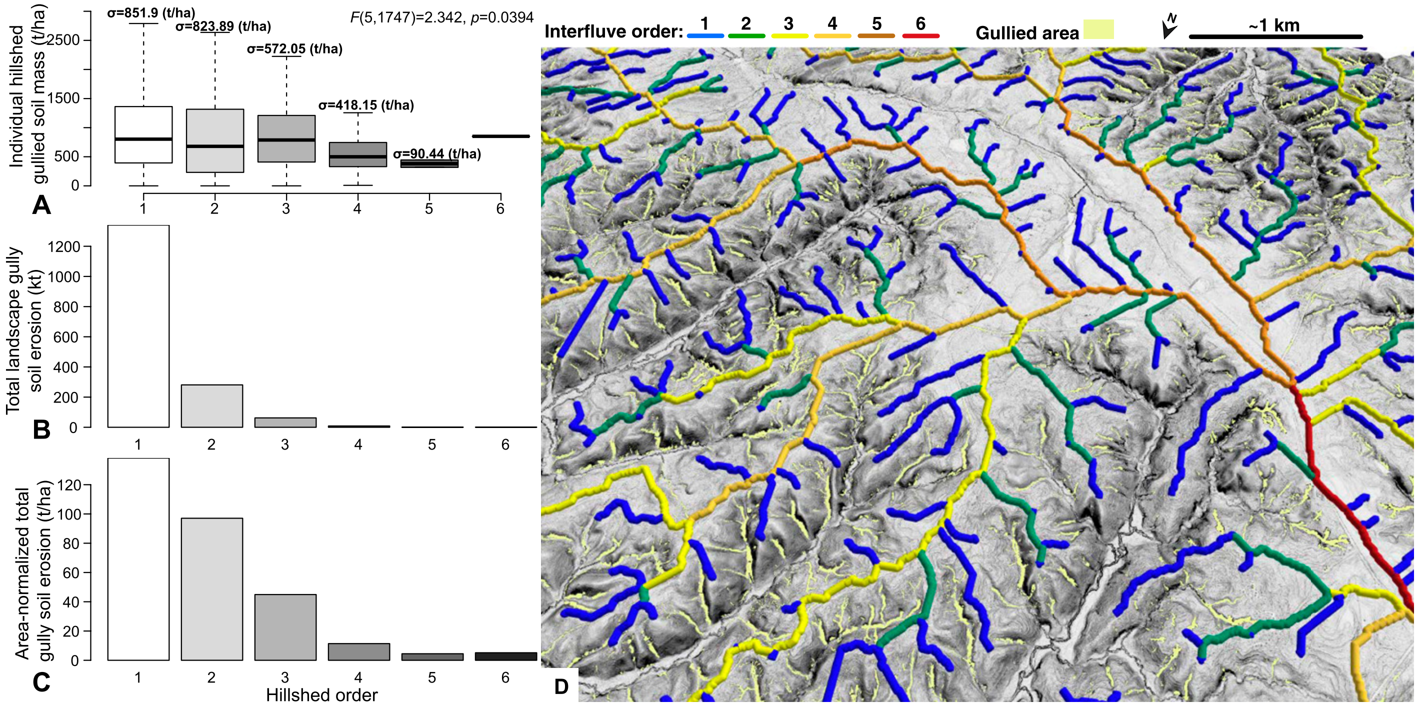

Figure 6. (A–C) Critical zone soil-erosion application plots of (A) individual hillshed gullied soil mass per hectare (t/ha) with analysis of variance (ANOVA) results, (B) cumulative historic gully-erosion volumes across interfluve-hillshed orders in kilotons, and (C) area-normalized cumulative historic gully-erosion volumes across interfluve-hillshed orders in tons per hectare. (D) Aerial three-dimensional view of the Calhoun Critical Zone Observatory (CZO) topography with gullied areas highlighted and overlain by ordered interfluves. Image is centered approximately on –81.72° longitude and 34.62° latitude.

were mapped in the field and modeled by St. Clair et al. (2015). The bottom extent of weathering bedrock was modeled in three dimensions spatially as the boundary of the least compressive stress value of 0.5 MPa (gray bottom boundary in Fig. 7A) from Moon et al. (2017). This boundary corresponds to a seismic velocity contour of ~4 km/s, reflecting a transition from competent bedrock to fractured regolith (St. Clair et al., 2015). Results indicate that first-order hillsheds appear to have the greatest maximum modeled weathering depth (~53 m) and the highest spatial variability in regolith depth (Fig. 7B) as a function of higher topographic curvature or "pinching" in first- order hillsheds (Fig. 7A), with densely packed interfluve hilltops and stream valley bottoms (Anderson, 2015; Moon et al., 2017). Overall, however, the average regolith depth is remarkably similar across hillslope orders, with a tendency to be slightly shallower but much less variable as hillshed order increases—a function of the characteristic slopes and breadths of hillshed orders. This relationship is attributed to the high curvature of the steep and relatively narrow first-order hillsheds that perturb subsurface stress fields and produce spatially variable weathering depths mirroring the "pinched topography" across these hillsheds (Anderson, 2015; Moon et al., 2017; St. Clair et al., 2015).

Hillshed-Order Connections as Drivers of Landscape Geomorphology

Terrain analyses also demonstrated that hillshed characteristics depend on the order of the hillshed to which they connect. Figures 8A–8F thus illustrate how a hillshed's characteristics vary, especially those of first order, depending on whether its interfluve branches from a second-, third-, fourth-, fifth-, or sixth-order interfluve. In terms of abundance, low-order hillsheds that connect to low-order hillsheds (e.g., 123 or 234) are most abundant within their order (e.g., first or second order; Fig. 8A). Hillshed abundance decreases with increasing hillshed order and with increasing interfluve branching order (e.g., 560 or 160 vs. 123 or 234). Individual hillshed areas remain fairly consistent within their single-digit orders regardless of the hillshed orders from which they branch (Fig. 8B). For example, all types of first-order hillsheds (i.e., hillshed orders 123 through 160) tend to be smaller in area than the second-order hillsheds (i.e., hillshed orders 234 through 260), which tend to be smaller than the third-order hillsheds, etc., though variability is high. "Main-stem" hillshed orders like 123, 234, 456, etc., account for ~56% of the upland area across the Calhoun CZO, though they only represent six of the twenty five possible branching sequences found across the Calhoun CZO (Fig. 8C).

The steepest and narrowest hillsheds are low order with the lowest elevation and are furthest in distance from the geomorphic trunks of the landscape. Though there is much variability, the relationships of elevation and its derivatives, slope and curvature, show that proximity to fifth- and sixth-order trunks in the landscape influences landscape geomorphology. Proximity to fifth- and sixth-order hillsheds is associated with increased elevation (Fig. 8D) ($F[24,1392] = 72.12$, $p < 0.05$), decreased slope ($F[24,1392] = 16.12$, $p < 0.05$), and decreased curvature ($F[24,1392] = 8.94$, $p < 0.05$) within hillsheds most closely joined to high-order hillsheds (e.g., 156 or 256; Figs. 8E–8F). Considered together, three-digit hillshed slopes and elevations help to characterize dynamic long-term landscape evolution as studied and modeled in studies like those of Scherler and Schwanghart (2020a, 2020b), Perron (2009), and Perron et al. (2017).

A comparison of multiple regression analyses further demonstrated the utility of

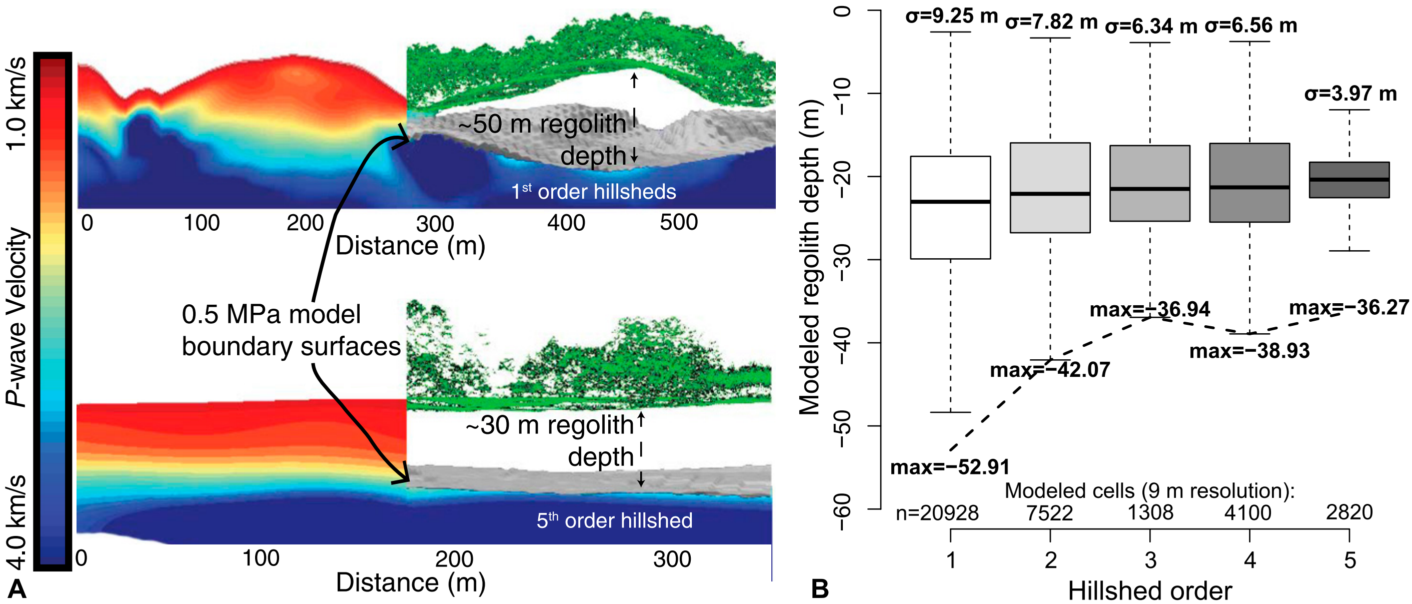

Figure 7. (A) Critical zone application diagram of weathered regolith profile shown along horizontal transects on first-order (top) and fifth-order (bottom) hillsheds. Two-dimensional field measurements of P-wave velocity profiles are shown as heat maps (modified from St. Clair et al., 2015) for the left half of the transects, with blue shades representing unfractured bedrock. On the right side is the modeled surface with the regolith volume (fractured rock and soil) cleared out (white space) above the three-dimensional modeled 0.5 MPa boundary surface in gray. Blue color was retained below the gray surface to maintain continuity between the two sides of panel A. Gray bottom boundary of the 0.5 MPa modeled regolith depth from Moon et al. (2017) is located along the transition from fractured regolith to unfractured bedrock and was computed by least compressive stress modeling corresponding well with a P-wave velocity of ~4 km/s. The modeled regolith maximum depth surface is plotted below green-colored light detection and ranging (LiDAR) point clouds highlighting vegetation and the ground surface for the right half of both transects. (B) Regolith depth distribution box plots of modeled regolith depths within Holcombe's Branch for hillshed orders 1, 2, 3, 4, and 5. Standard deviations of modeled weathering depth values are shown for each order above the upper whisker, and maximum modeled regolith depths are plotted and labeled along a dashed line.

multiple-digit ordering of hillsheds. Figure 9 plots median elevation for each ordered hillshed alongside median hillshed slope and hillshed area. Multiple regression modeling of hillshed elevation as a function of hillshed single-digit order, hillshed slope, and hillshed area, though statistically significant, showed low explanatory power (adjusted $R^2 = 0.15$, $F[7,1409] = 36.66$, $p < 0.05$). A low ability to model landscape elevation as a function of slope and area is perhaps not surprising given the high variability of both median elevation and slope values for first- and second-order hillsheds. However, by including the three-digit interfluve-branching hillshed order as a predictive factor in the analysis instead of the single-digit order, the explanatory power of the model was greatly enhanced (adjusted $R^2 = 0.55$, $F[26,1390] = 68.9$, $p < 0.05$). The increase in model R^2 and F statistics reflects the importance of local interfluve-hillshed network connections in landscape geomorphology by partitioning within-order variation among branching sequences to further emphasize upslope versus downslope position across the landscape. Hillsheds situated furthest from sixth- or fifth-order interfluve trunks of the landscape are lower in elevation than those more proximal to high-order hillsheds. Hillsheds that are two branching junctions downslope from sixth-, fifth-, fourth-, or third-order interfluves (i.e., ##6, ##5, ##4, or 123) are, on average, 6 m, 16 m, 29 m, or 44 m lower, respectively, in median elevation than hillsheds that are either sixth order or immediately branch from a sixth-order interfluve (i.e., 600 or #60; Fig. 8D).

CONCLUSIONS

The hillshed ordering approach developed here provides a geomorphic framework that can advance the science and management of landscapes as critical zones. This is accomplished not by point-grid examinations of landscapes according to elevation, slope, or curvature alone, but by initially and hierarchically networking interfluves and subsequently delineating their respective hillsheds through which all terrain attributes can be considered concurrently. We recognize the potential and need for advancement and improvement of automated interfluve network extraction process, paired with hillshed delineation. Our method relied on a series of heuristic flow-accumulation thresholds on inverted terrain that likely do not lend themselves well to universal application of methodology in contrasting landscapes. Our goal in this study, however, was to demonstrate how understanding the spatial distribution of ordered hillshed geomorphology enhances our ability to link 3-D landscape structure to critical zone function. This was illustrated by terrain metrics, land-cover change over decades and centuries, intensity of gully erosion from historic agriculture, depth of potential rock weathering, and the importance of interfluve branching and connections in the geomorphic evolution of hillsheds across landscapes. Many processes such as soil formation, landscape evolution, groundwater storage, catchment hydrologic responses, mobile-regolith production and movement via soil creep, biologic productivity, management sustainability, and even processes like fire behavior (Bos, 1971; Sullivan et al., 2014)

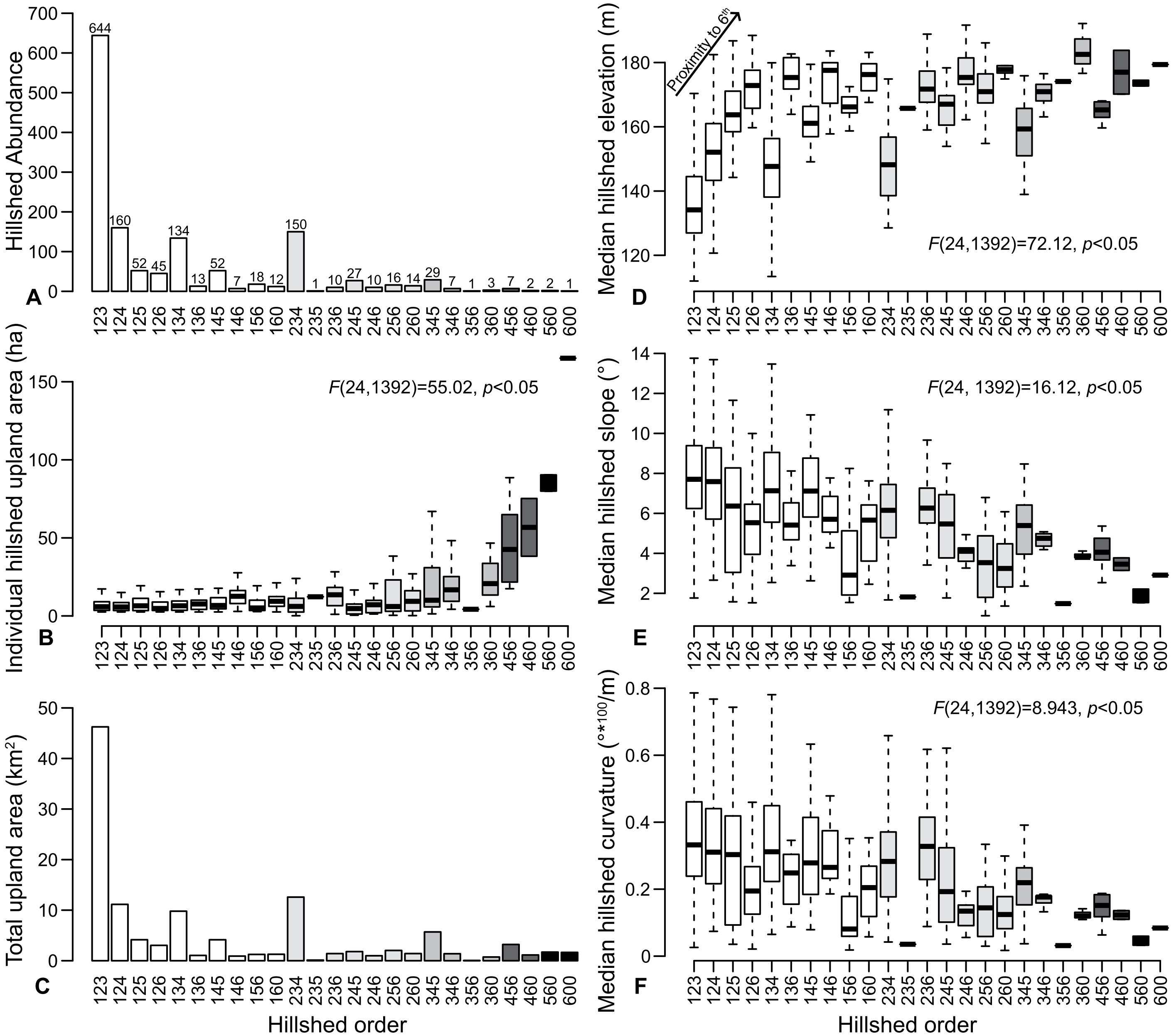

Figure 8. Three-digit interfluve ordering terrain analyses of hillshed: (A) abundance, (B) area, (C) cumulative area, (D) median elevation, (E) median slope, and (F) median hillshed total curvature (Lindsay, 2019). The number of interfluves in each order is above each bar in the top abundance panel, and analysis of variance (ANOVA) *F*-test results are shown within area, elevation, slope, and curvature box plots. The first digit corresponds to the interfluve order, and the second and third digits correspond to the first and second orders of the interfluve junctions uphill.

may be related to the geomorphic attributes of interfluves and their hillsheds. These processes span the disciplines of geomorphology, environmental history and anthropology, biogeochemistry, geophysics, hydrology, remote sensing, soil science, ecology, and land and water management.

Ordered interfluves and hillsheds can help to structure future scientific investigation of landscapes and frame statistical analyses, providing a geomorphic organization that spans spatial and temporal scales and thus advances research and management of critical zones. The Southern Piedmont in the United States is often described as having "gently rolling hills" or "undulating topography." While true, the topography of regions like the Calhoun CZO is not a random occurrence of hills and dales (Maxwell, 1870). The topography in this setting, and likely a great many more, has organized patterns that result from landform evolution over multiple millennia, shaped by weathering, erosion, human activity and conditioned by underlying bedrock, biota, and climate (Gilbert, 1877; Jenny, 1994; Perron et al., 2009). Future terrain analyses of interfluve and hillshed orders will examine landscapes that contrast with those at the ancient and deeply weathered Calhoun CZO to further explore interfluve, hillshed, and environmental process relations.

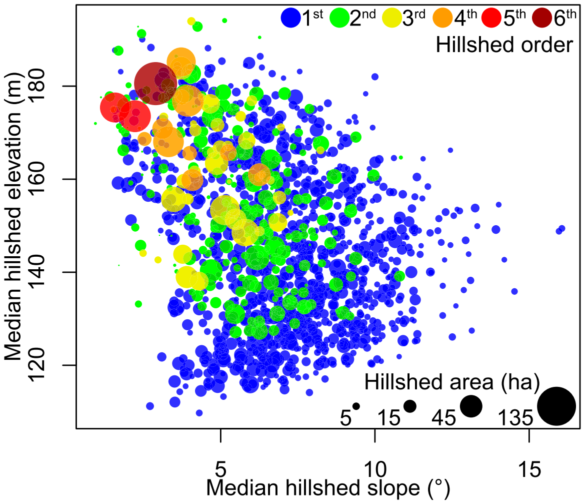

Figure 9. Scatterplot of interfluve-ordered hillshed median elevation and median slope. The size of points corresponds to the areas of individual hillsheds, and the color corresponds to the hillshed order.

ACKNOWLEDGMENTS

This work was supported by the National Science Foundation (NSF) through support for the Calhoun Critical Zone Observatory (EAR1331846) to D.D. Richter, NSF Integrative Graduate Education and Research Traineeship (IGERT; DGE-1068871) and the Forest History Society Weyerhaeuser Fellowship to Z.S. Brecheisen, and NSF grants (EAR1945431) and (EAR 2012073) to S. Moon. We would like to thank Steve Holbrook, Mukesh Kumar, and William E. Dietrich for their advice and feedback at various stages of this project. Thanks are also due to Jay Austin, Will Cook, Daniel Markewitz, Paul Schroeder, Terry Ferguson, Peter Haff, Michael Coughlan, Don Nelson, Allan James, John Mallard, Brian McGlynn, and Mark River for conversations in the field and around many campfires over the years that advanced the thinking and work that have gone into this manuscript. Last, much gratitude is owed to the editors and reviewers, whose thorough consideration and insightful recommendations have greatly elevated this study.

REFERENCES CITED

Anderson, R.S., 2015, Pinched topography initiates the critical zone: Geophysical imaging provides a clearer picture of how rock turns into soil: Science, v. 350, no. 6260, p. 506–507, https://doi.org/10.1126/science.aad2266.

Anderson, R.S., Anderson, S.P., and Tucker, G.E., 2013, Rock damage and regolith transport by frost: An example of climate modulation of the geomorphology of the critical zone: Earth Surface Processes and Landforms, v. 38, no. 3, p. 299–316, https://doi.org/10.1002/esp.3330.

Bacon, A.R., Richter, D.D., Bierman, P.R., and Rood, D.H., 2012, Coupling meteoric ^{10}Be with pedogenic losses of ^{9}Be to improve soil residence time estimates on an ancient North American interfluve: Geology, v. 40, no. 9, p. 847–850, https://doi.org/10.1130/G33449.1.

Befus, K.M., Sheehan, A.F., Leopold, M., Anderson, S.P., and Anderson, R.S., 2011, Seismic constraints on critical zone architecture, Boulder Creek watershed, Front Range, Colorado: Vadose Zone Journal, v. 10, no. 3, p. 915–927, https://doi.org/10.2136/vzj2010.0108.

Bos, R.H.G., 1971, Quaternary Evolution of a Mountainous Area in N.W. Tunisia: A Geomorphological and Pedological Analysis: Amsterdam, Netherlands, Universiteit van Amsterdam, 167 p.

Brantley, S.L., Goldhaber, M.B., and Ragnarsdottir, K.V., 2007, Crossing disciplines and scales to understand the critical zone: Elements, v. 3, no. 5, p. 307–314, https://doi.org/10.2113/gselements.3.5.307.

Brantley, S.L., DiBiase, R.A., Russo, T.A., Shi, Y., Lin, H., Davis, K.J., Kaye, M., Hill, L., Kaye, J., Eissenstat, D.M., Hoagland, B., Dere, A.L., Neal, A.L., Brubaker, K.M., and Arthur, D.K., 2016, Designing a suite of measurements to understand the critical zone: Earth Surface Dynamics, v. 4, no. 1, p. 211–235, https://doi.org/10.5194/esurf-4-211-2016.

Brecheisen, Z.S., and Richter, D.D., 2021, Gully-erosion estimation and terrain reconstruction using analyses of microtopographic roughness and LiDAR: Catena, v. 202, 105264, https://doi.org/10.1016/j.catena.2021.105264.

Brecheisen, Z., Cook, C., and Harmon, M., 2019a, CCZO–GIS/Map Data, Photographic Imagery—1933 Aerial Imagery Composite–Calhoun Experimental Forest, SC–(1933–1933): Hydroshare, http://www.hydroshare.org/resource/3edb9720a11845169dae4ba5b6212d27 (accessed 1 January 2020).

Brecheisen, Z.S., Cook, C.W., Heine, P.R., and Richter, D.D., 2019b, Micro-topographic roughness analysis (MTRA) highlights minimally eroded terrain in a landscape severely impacted by historic agriculture: Remote Sensing of Environment, v. 222, p. 78–89, https://doi.org/10.1016/j.rse.2018.12.025.

Calhoun Critical Zone Observatory (CCZO), 2014, Leaf-On LiDAR Survey of the Calhoun Critical Zone Observatory: OpenTopography, National Center for Airborne Laser Mapping, https://portal.opentopography.org/datasetMetadata?otCollectionID=OT.122015.26917.1 (accessed 1 January 2020).

Callow, J., Van Niel, K., and Boggs, G., 2007, How does modifying a DEM to reflect known hydrology affect subsequent terrain analysis?: Journal of Hydrology (Amsterdam), v. 332, p. 30–39, https://doi.org/10.1016/j.jhydrol.2006.06.020.

Cayley, A., 1859, On contour and slope lines: The Philosophical Magazine and Journal of Science, v. 18, p. 264–268, https://doi.org/10.1080/14786445908642760.

Chang, Y.-C., and Frigeri, A., 2002, Implementing the automatic extraction of ridge and valley axes using the PPA algorithm in Grass GIS: Open-Source GIS–GRASS users conference: Trento, Italy, https://www.researchgate.net/profile/Alessandro-Frigeri/publication/228414474_Implementing_the_automatic_extraction_of_ridge_and_valley_axes_using_the_PPA_algorithm_in_Grass_GIS/links/0fcfd50ca4af908ea6000000/Implementing-the-automatic-extraction-of-ridge-and-valley-axes-using-the-PPA-algorithm-in-Grass-GIS.pdf (accessed 1 January 2018).

Chang, Y.-C., Song, G.-S., and Hsu, S.-K., 1998, Automatic extraction of ridge and valley axes using the profile recognition and polygon-breaking algorithm: Computers & Geosciences, v. 24, no. 1, p. 83–93, https://doi.org/10.1016/S0098-3004(97)00078-2.

Chorover, J., Troch, P.A., Rasmussen, C., Brooks, P.D., Pelletier, J.D., Breshears, D.D., Huxman, T.E., Kurc, S.A., Lohse, K.A., McIntosh, J.C., Meixner, T., Schaap, M.G., Litvak, M.E., Perdrial, J., Harpold, A., and Durcik, M., 2011, How water, carbon, and energy drive critical zone evolution: The Jemez–Santa Catalina Critical Zone Observatory: Vadose Zone Journal, v. 10, no. 3, p. 884–899, https://doi.org/10.2136/vzj2010.0132.

Conrad, O., Bechtel, B., Bock, M., Dietrich, H., Fischer, E., Gerlitz, L., Wehberg, J., Wichmann, V., and Böhner, J., 2015, System for Automated Geoscientific Analyses (SAGA) v. 2.1.4: Geoscientific Model Development, v. 8, no. 7, p. 1991–2007, https://doi.org/10.5194/gmd-8-1991-2015.

Coughlan, M., Nelson, D., Lonneman, M., and Block, A., 2017, Historical land use dynamics in the highly degraded landscape of the Calhoun Critical Zone Observatory: Land (Basel), v. 6, no. 2, p. 32, https://doi.org/10.3390/land6020032.

Čučković, Z., 2016, Creation and analysis of topographic (surface) networks, *in* Topographic Networks: QGIS Python Plugins Repository, https://plugins.qgis.org/plugins/TopographicNetworks/ (accessed 1 January 2017).

Deng, Y., Wilson, J.P., and Bauer, B.O., 2007, DEM resolution dependencies of terrain attributes across a landscape: International Journal of Geographical Information Science, v. 21, no. 2, p. 187–213, https://doi.org/10.1080/13658810600894364.

Dialynas, Y., Bastola, S., Bras, R., Billings, S., Markewitz, D., and Richter, D., 2016, Topographic variability and the influence of soil erosion on the carbon cycle: Global Biogeochemical Cycles, v. 30, no. 5, p. 644–660, https://doi.org/10.1002/2015GB005302.

Dietrich, W.E., Wilson, C.J., Montgomery, D.R., McKean, J., and Bauer, R., 1992, Erosion thresholds and land surface morphology: Geology, v. 20, no. 8, p. 675–679, https://doi.org/10.1130/0091-7613(1992)020<0675:ETALSM>2.3.CO;2.

ESRI, 2016, ArcGIS Desktop: Release 10.5: ESRI, https://desktop.arcgis.com/en/quick-start-guides/10.5/arcgis-desktop-quick-start-guide.htm (accessed 1 January 2018).

Evans, I.S., 2012, Geomorphometry and landform mapping: What is a landform?: Geomorphology, v. 137, no. 1, p. 94–106, https://doi.org/10.1016/j.geomorph.2010.09.029.

Evans, I.S., and Cox, N.J., 1999, Relations between land surface properties: Altitude, slope and curvature, *in* Hergarten, S., and Neugebauer, H.J., eds., Process Modelling and Landform Evolution: Berlin, Springer, Lecture Notes in Earth Sciences 78, https://doi.org/10.1007/BFb0009718.

Fernandes, N.F., and Dietrich, W.E., 1997, Hillslope evolution by diffusive processes: The timescale for equilibrium adjustments: Water Resources Research, v. 33, no. 6, p. 1307–1318, https://doi.org/10.1029/97WR00534.

Flinchum, B.A., Steven Holbrook, W., Rempe, D., Moon, S., Riebe, C.S., Carr, B.J., Hayes, J.L., St. Clair, J., and Peters, M.P., 2018, Critical zone structure under a granite ridge inferred from drilling and three-dimensional seismic refraction data: Journal of Geophysical Research–Earth Surface, v. 123, no. 6, p. 1317–1343, https://doi.org/10.1029/2017JF004280.

Giesen, J.C., 2020, The view from Rose Hill: Environmental, architectural, and cultural recovery on a piedmont landscape: Buildings and Landscapes, v. 27, no. 2, p. 19–38, https://doi.org/10.5749/buildland.27.2.0019.

Gilbert, G.K., 1877, Geology of the Henry Mountains: Washington, D.C., Government Printing Office, https://doi.org/10.3133/70038096.

Godsey, S.E., Marks, D., Kormos, P.R., Seyfried, M.S., Enslin, C.L., Winstral, A.H., McNamara, J.P., and Link, T.E., 2018, Eleven years of mountain weather, snow, soil moisture and streamflow data from the rain-snow transition zone—The Johnston Draw catchment, Reynolds Creek Experimental Watershed and Critical Zone Observatory, USA: Earth System Science Data, v. 10, no. 3, p. 1207, https://doi.org/10.5194/essd-10-1207-2018.

GRASS Development Team, 2017, Geographic Resources Analysis Support System (GRASS) Software: Open Source Geospatial Foundation, http://grass.osgeo.org/ (accessed 1 January 2018).

Grieve, S.W.D., Mudd, S.M., Milodowski, D.T., Clubb, F.J., and Furbish, D.J., 2016, How does grid-resolution modulate the topographic expression of geomorphic processes?: Earth Surface Dynamics, v. 4, no. 3, p. 627–653, https://doi.org/10.5194/esurf-4-627-2016.

Hansen, W.F., 1991, Land rehabilitation on the Sumter National Forest, *in* Furniss, M., Clifton, C., and Ronnenberg, K., eds., Advancing the Fundamental Sciences: Proceedings of the Forest Service National Earth Sciences Conference, San Diego, California, 18–22 October 2004, PNWGTR-689: Portland, Oregon, U.S. Department of Agriculture, Forest Service, Pacific Northwest Research Station.

Happ, S., 1945, Sedimentation in South Carolina Piedmont valleys: American Journal of Science, v. 243, no. 3, p. 113–126, https://doi.org/10.2475/ajs.243.3.113.

Hasenmueller, E.A., Gu, X., Weitzman, J.N., Adams, T.S., Stinchcomb, G.E., Eissenstat, D.M., Drohan, P.J., Brantley, S.L., and Kaye, J.P., 2017, Weathering of rock to regolith: The activity of deep roots in bedrock fractures: Geoderma, v. 300, p. 11–31, https://doi.org/10.1016/j.geoderma.2017.03.020.

Hesselbarth, M.H.K., Sciaini, M., With, K.A., Wiegand, K., and Nowosad, J., 2019, Landscapemetrics: An open-source R tool to calculate landscape metrics: Ecography, v. 42, p. 1648–1657, https://doi.org/10.1111/ecog.04617.

Hijmans, R.J., 2020, raster: Geographic data analysis and modeling, https://CRAN.R-project.org/package=raster (accessed 1 November 2020).

Hodges, C., Mallard, J., Markewitz, D., Barcellos, D., and Thompson, A., 2019, Seasonal and spatial variation in the potential for iron reduction in soils of the southeastern Piedmont of the US: Catena, v. 180, p. 32–40, https://doi.org/10.1016/j.catena.2019.03.026.

Holbrook, W.S., Riebe, C.S., Elwaseif, M., Hayes, J.L., Basler-Reeder, K., Harry, D.L., Malazian, A., Dosseto, A., Hartsough, P.C., and Hopmans, J.W., 2014, Geophysical constraints on deep weathering and water storage potential in the Southern Sierra Critical Zone Observatory: Earth Surface Processes and Landforms, v. 39, no. 3, p. 366–380, https://doi.org/10.1002/esp.3502.

Holbrook, W.S., Marcon, V., Bacon, A.R., Brantley, S.L., Carr, B.J., Flinchum, B.A., Richter, D.D., and Riebe, C.S., 2019, Links between physical and chemical weathering inferred from a 65-m-deep borehole through Earth's critical zone: Scientific Reports, v. 9, no. 1, p. 4495, https://doi.org/10.1038/s41598-019-40819-9.

Homer, C.G., Dewitz, J.A., Yang, L., Jin, S., Danielson, P., Xian, G., Coulston, J., Herold, N.D., Wickham, J.D., and Megown, K., 2015, Completion of the 2011 National Land Cover Database for the conterminous United States—Representing a decade of land cover change information: Photogrammetric Engineering and Remote Sensing, v. 81, no. 5, p. 345–354.

Horton, R.E., 1945, Erosional development of streams and their drainage basins: Hydrophysical approach to quantitative morphology: Geological Society of America Bulletin, v. 56, no. 3, p. 275–370, https://doi.org/10.1130/0016-7606(1945)56[275:EDOSAT]2.0.CO;2.

James, L.A., 2013, Legacy sediment: Definitions and processes of episodically produced anthropogenic sediment: Anthropocene, v. 2, p. 16–26, https://doi.org/10.1016/j.ancene.2013.04.001.

Jenny, H., 1994, Factors of Soil Formation: A System of Quantitative Pedology: New York, McGraw-Hill Book Company (reprinted by Dover), 281 p.

Lebedeva, M.I., and Brantley, S.L., 2013, Exploring geochemical controls on weathering and erosion of convex hillslopes: Beyond the empirical regolith production function: Earth Surface Processes and Landforms, v. 38, no. 15, p. 1793–1807, https://doi.org/10.1002/esp.3424.

Lehner, B., and Grill, G., 2013, Global river hydrography and network routing: Baseline data and new approaches to study the world's large river systems: Hydrological Processes, v. 27, no. 15, p. 2171–2186, https://doi.org/10.1002/hyp.9740.

Lindsay, J., 2019, WhiteboxTools User Manual: Guelph, Ontario, Canada, University of Guelph Geomorphometry and Hydrogeomatics Research Group, https://www.whiteboxgeo.com/manual/wbt_book/intro.html (accessed 1 January 2019).

Lindsay, J.B., 2016, The practice of DEM stream burning revisited: Earth Surface Processes and Landforms, v. 41, no. 5, p. 658–668, https://doi.org/10.1002/esp.3888.

Mark, D.M., 1979, Topology of ridge patterns: Randomness and constraints: Geological Society of America Bulletin, v. 90, p. 164–172, https://doi.org/10.1130/0016-7606(1979)90<164:TORPRA>2.0.CO;2.

Mark, D.M., and Smith, B., 2004, A science of topography: From qualitative ontology to digital representations, *in* Bishop, M.P., and Shroder, J.F., eds., Geographic Information Science and Mountain Geomorphology: Chichester, UK, Springer-Praxis, p. 75–100.

Maxwell, J.C., 1870, On hills and dales: Philosophical Magazine, v. 4, p. 421–427.

Meade, R.H., 1982, Sources, sinks, and storage of river sediment in the Atlantic drainage of the United States: The Journal of Geology, v. 90, no. 3, p. 235–252, https://doi.org/10.1086/628677.

Meade, R.H., and Trimble, S.W., 1974, Changes in sediment loads in rivers of the Atlantic drainage of the United States since 1900, *in* Effects of Man on the Interface of the Hydrological Cycle with the Physical Environment: International Association of Hydrological Sciences Special Publication 103, p. 99–104.

Meerveld, I.T.-v., and Weiler, M., 2008, Hillslope dynamics modeled with increasing complexity: Journal of Hydrology (Amsterdam), v. 361, no. 1–2, p. 24–40, https://doi.org/10.1016/j.jhydrol.2008.07.019.

Metz, L.J., 1958, The Calhoun Experimental Forest, Asheville, NC: USDA Forest Service Southeastern Forest Experiment Station, https://doi.org/10.5962/bhl.title.115583.

Montgomery, D.R., 1999, Process domains and the river continuum: Journal of the American Water Resources Association, v. 35, no. 2, p. 397–410, https://doi.org/10.1111/j.1752-1688.1999.tb03598.x.

Montgomery, D.R., and Dietrich, W.E., 1992, Channel initiation and the problem of landscape scale: Science, v. 255, no. 5046, p. 826–830, https://doi.org/10.1126/science.255.5046.826.

Moon, S., Perron, J.T., Martel, S.J., Holbrook, W.S., and St. Clair, J., 2017, A model of three-dimensional topographic stresses with implications for bedrock fractures, surface processes, and landscape evolution: Journal of Geophysical Research–Earth Surface, v. 122, no. 4, p. 823–846, https://doi.org/10.1002/2016JF004155.

Noto, L.V., Bastola, S., Dialynas, Y.G., Arnone, E., and Bras, R.L., 2017, Integration of fuzzy logic and image analysis for the detection of gullies in the Calhoun Critical Zone Observatory using airborne LiDAR data: ISPRS Journal of Photogrammetry and Remote Sensing, v. 126, p. 209–224, https://doi.org/10.1016/j.isprsjprs.2017.02.013.

Perron, J.T., 2017, Climate and the pace of erosional landscape evolution: Annual Review of Earth and Planetary Sciences, v. 45, p. 561–591, https://doi.org/10.1146/annurev-earth-060614-105405.

Perron, J.T., Kirchner, J.W., and Dietrich, W.E., 2009, Formation of evenly spaced ridges and valleys: Nature, v. 460, no. 7254, p. 502–505, https://doi.org/10.1038/nature08174.

Pfaltz, J.L., 1976, Surface networks: Geographical Analysis, v. 8, no. 1, p. 77–93, https://doi.org/10.1111/j.1538-4632.1976.tb00530.x.

Purinton, B., and Bookhagen, B., 2017, Validation of digital elevation models (DEMs) and comparison of geomorphic metrics on the southern Central Andean Plateau: Earth Surface Dynamics, v. 5, no. 2, p. 211–237, https://doi.org/10.5194/esurf-5-211-2017.

QGIS Development Team, 2016, QGIS Geographic: Information Systems, https://qgis.org/en/site/ (accessed 1 January 2018).

R Core Team, 2020, R: A Language and Environment for Statistical Computing: Vienna, Austria, R Foundation for Statistical Computing.

Rempe, D.M., and Dietrich, W.E., 2014, A bottom-up control on fresh-bedrock topography under landscapes: Proceedings of the National Academy of Sciences of the United States of America, v. 111, no. 18, p. 6576–6581, https://doi.org/10.1073/pnas.1404763111.

Richter, D., and Billings, S.A., 2015, 'One physical system': Tansley's ecosystem as Earth's critical zone: The New Phytologist, v. 206, no. 3, p. 900–912, https://doi.org/10.1111/nph.13338.

Richter, D.D., Jr., and Markewitz, D., 2001, Understanding Soil Change: Soil Sustainability Over Millennia, Centuries, and Decades: Cambridge, Cambridge University Press, 272 p.

Riebe, C.S., Hahm, W.J., and Brantley, S.L., 2017, Controls on deep critical zone architecture: A historical review and four testable hypotheses: Earth Surface Processes and Landforms, v. 42, no. 1, p. 128–156, https://doi.org/10.1002/esp.4052.

Rodriguez, F., Maire, E., Courjault-Radé, P., and Darrozes, J., 2002, The Black Top Hat function applied to a DEM: A tool to estimate recent incision in a mountainous watershed: Geophysical Research Letters, v. 26, no. 9, p. 9-1–9-4, https://doi.org/10.1029/2001GL014412.

Ross, N., 2020, fasterize: Fast Polygon to Raster Conversion, https://cran.r-project.org/web/packages/fasterize/index.html (accessed 1 January 2020).

Ruhe, R., Daniels, R., and Cady, J., 1967, Landscape Evolution and Soil Formation in Southwestern Iowa: Soil Conservation Service, U.S. Department of Agriculture Technical Bulletin 1349, 242 p.

Scherler, D., and Schwanghart, W., 2020a, Drainage divide networks—Part 1: Identification and ordering in digital elevation models: Earth Surface Dynamics, v. 8, p. 245–259, https://doi.org/10.5194/esurf-8-245-2020.

Scherler, D., and Schwanghart, W., 2020b, Drainage divide networks—Part 2: Response to perturbations: Earth Surface Dynamics, v. 8, no. 2, p. 261–274, https://doi.org/10.5194/esurf-8-261-2020.

Schneider, B., 2005, Extraction of hierarchical surface networks from bilinear surface patches: Geographical Analysis, v. 37, p. 244–263, https://doi.org/10.1111/j.1538-4632.2005.00638.x.

Seyfried, M., Lohse, K., Marks, D., Flerchinger, G., Pierson, F., and Holbrook, W.S., 2018, Reynolds Creek Experimental Watershed and Critical Zone Observatory: Vadose Zone Journal, v. 17, no. 1, p. 1–20, https://doi.org/10.2136/vzj2018.07.0129.

St. Clair, J., Moon, S., Holbrook, W.S., Perron, J.T., Riebe, C.S., Martel, S.J., Carr, B., Harman, C., Singha, K., and Richter, D., 2015, Geophysical imaging reveals topographic stress control of bedrock weathering: Science, v. 350, no. 6260, p. 534–538, https://doi.org/10.1126/science.aab2210.

Strahler, A.N., 1957, Quantitative analysis of watershed geomorphology: Eos (Washington, D.C.), v. 38, no. 6, p. 913–920.

Sullivan, A.L., Sharples, J.J., Matthews, S., and Plucinski, M.P., 2014, A downslope fire spread correction factor based on landscape-scale fire behaviour: Environmental Modelling & Software, v. 62, p. 153–163, https://doi.org/10.1016/j.envsoft.2014.08.024.

Tarboton, D.G., 1996, Fractal river networks, Horton's laws and Tokunaga cyclicity: Journal of Hydrology (Amsterdam), v. 187, p. 105–117, https://doi.org/10.1016/S0022-1694(96)03089-2.

Tarboton, D.G., 2015, Terrain Analysis Using Digital Elevation Models (TauDEM): Logan, Utah, Utah State University, https://hydrology.usu.edu/taudem/taudem5/ (accessed 1 January 2018).

Thomas, A.L., 1993, Poly3D: A Three-Dimensional, Polygonal Element, Displacement Discontinuity Boundary Element Computer Program with Applications to Fractures, Faults, and Cavities in the Earth's Crust: Stanford, California, Stanford University, 221 p.

Thorley, R.M., Taylor, L.L., Banwart, S.A., Leake, J.R., and Beerling, D.J., 2015, The role of forest trees and their mycorrhizal fungi in carbonate rock weathering and its significance for global carbon cycling: Plant, Cell & Environment, v. 38, no. 9, p. 1947–1961, https://doi.org/10.1111/pce.12444.

Thorp, J.H., and Delong, M.D., 1994, The riverine productivity model: An heuristic view of carbon sources and organic processing in large river ecosystems: Oikos, v. 70, no. 2, p. 305–308, https://doi.org/10.2307/3545642.

Trimble, S.W., 1975a, A volumetric estimate of man-induced erosion on the Southern Piedmont, *in* Present and Prospective Technology for Predictive Sediment Yields and Sources: U.S. Department of Agriculture, Agricultural Research Service Publication S40, p. 142–154.

Trimble, S.W., 1975b, Denudation studies: Can we assume steady state?: Science, v. 188, p. 1207–1208, https://doi.org/10.1126/science.188.4194.1207.

Trimble, S., 2008, Man-Induced Soil Erosion on the Southern Piedmont: Ankeny, Iowa, Soil and Water Conservation Society, 64 p.

Tucker, G., and Bras, R., 1998, Hillslope processes, drainage density, and landscape morphology: Water Resources Research, v. 34, no. 10, p. 2751–2764, https://doi.org/10.1029/98WR01474.

U.S. Fish & Wildlife Service, 1979–1994, National Wetlands Inventory Data: U.S. Fish & Wildlife Service, National Wetlands Inventory.

U.S. Forest Service (USFS), 2016, FSTopo Boundary Ownership Polygon: http://data.fs.usda.gov/geodata/edw/datasets.php (accessed 12 September 2021).

U.S. Geological Survey, 2002, The National Map—Hydrography: U.S. Geological Survey Fact Sheet 060-02, https://pubs.usgs.gov/fs/2002/0060/report.pdf.

Vannote, R.L., Minshall, G.W., Cummins, K.W., Sedell, J.R., and Cushing, C.E., 1980, The river continuum concept: Canadian Journal of Fisheries and Aquatic Sciences, v. 37, no. 1, p. 130–137, https://doi.org/10.1139/f80-017.

Veltri, P., Veltri, M., and Maiolo, M., 1996, On the fractal description of natural channel networks: Journal of Hydrology (Amsterdam), v. 187, no. 1, p. 137–144, https://doi.org/10.1016/S0022-1694(96)03091-0.

Wade, A.M., Richter, D.D., Cherkinsky, A., Craft, C.B., and Heine, P.R., 2020, Limited carbon contents of centuries old soils forming in legacy sediment: Geomorphology, v. 354, 107018, https://doi.org/10.1016/j.geomorph.2019.107018.

Walter, R.C., and Merritts, D.J., 2008, Natural streams and the legacy of water-powered mills: Science, v. 319, no. 5861, p. 299–304, https://doi.org/10.1126/science.1151716.

Warntz, W., 1975, Stream ordering and contour mapping: Journal of Hydrology (Amsterdam), v. 25, p. 209–227, https://doi.org/10.1016/0022-1694(75)90022-0.

Werner, C., 1972, Patterns of drainage areas with random topology: Geographical Analysis, v. 4, no. 2, p. 119–133, https://doi.org/10.1111/j.1538-4632.1972.tb00464.x.

Werner, C., 1988, Formal analysis of ridge and channel patterns in maturely eroded terrain: Annals of the Association of American Geographers, v. 78, no. 2, p. 253–270, https://doi.org/10.1111/j.1467-8306.1988.tb00206.x.

White, T., Brantley, S., Banwart, S., Chorover, J., Dietrich, W., Derry, L., Lohse, K., Anderson, S., Aufdendkampe, A., Bales, R., Kumar, P., Richter, D., and McDowell, B., 2015, The role of critical zone observatories in critical zone science, *in* Giardino, J.R., and Houser, C., eds., Principles and Dynamics of the Critical Zone: Amsterdam, Netherlands, Elsevier, Developments in Earth Surface Processes 19, p. 15–78, https://doi.org/10.1016/B978-0-444-63369-9.00002-1.

Wilcox, D., and Moellering, H., 1995, Pass location to facilitate the direct extraction of Warntz networks from grid digital elevation models, *in* Proceedings of the 12th International Symposium on Computer-Assisted Cartography: Charlotte, North Carolina, American Congress on Surveying and Mapping & American Society for Photogrammetry and Remote Sensing, p. 22–31.

Wymore, A.S., West, N.R., Maher, K., Sullivan, P.L., Harpold, A., Karwan, D., Marshall, J.A., Perdrial, J., Rempe, D.M., and Ma, L., 2017, Growing new generations of critical zone scientists: Earth Surface Processes and Landforms, v. 42, no. 14, p. 2498–2502, https://doi.org/10.1002/esp.4196.

Science Editor: Rob Strachan
Associate Editor: Emmanuel Gabet

Manuscript Received 16 April 2020
Revised Manuscript Received 1 August 2021
Manuscript Accepted 13 September 2021

Printed in the USA